Experimental investigation of residual ultimate strength of damaged metallic pipelines

Cai, Jie; Jiang, Xiaoli; Lodewijks, Gabriel; Pei, Zhiyong; Zhu, Ling

Important note
To cite this publication, please use the final published version (if applicable).
Please check the document version above.

Jie Cai[1]
Department of Maritime and
Transport Technology,
Delft University of Technology,
Delft 2628 CD, The Netherlands
e-mail: J.Cai-2@tudelft.nl

Xiaoli Jiang
Department of Maritime and
Transport Technology,
Delft University of Technology,
Delft 2628 CD, The Netherlands
e-mail: X.Jiang@tudelft.nl

Gabriel Lodewijks
Professor
School of Aviation,
University of New South Wales,
Sydney 2052, NSW, Australia
e-mail: g.lodewijks@unsw.edu.au

Zhiyong Pei
Departments of Naval Architecture,
Ocean and Structural Engineering,
School of Transportation,
Wuhan University of Technology,
Wuhan, China
e-mail: 15827146278@163.com

Ling Zhu
Professor
Departments of Naval Architecture,
Ocean and Structural Engineering,
School of Transportation,
Wuhan University of Technology,
Wuhan, China
e-mail: ZL79111@126.com

Experimental Investigation of Residual Ultimate Strength of Damaged Metallic Pipelines

The ultimate strength of metallic pipelines will be inevitably affected when they have suffered from structural damage after mechanical interference. The present experiments aim to investigate the residual ultimate bending strength of metallic pipes with structural damage based on large-scale pipe tests. Artificial damage, such as a dent, metal loss, a crack, and combinations thereof, is introduced to the pipe surface in advance. Four-point bending tests are performed to investigate the structural behavior of metallic pipes in terms of bending moment–curvature diagrams, failure modes, bending capacity, and critical bending curvatures. Test results show that the occurrence of structural damage on the pipe compression side reduces the bending capacity significantly. Only a slight effect has been observed for pipes with damage on the tensile side as long as no fracture failure appears. The possible causes that have introduced experimental errors are presented and discussed. The test data obtained in this paper can be used to further quantify damage effects on bending capacity of seamless pipes with similar D/t ratios. The comparison results in this paper can facilitate the structural integrity design as well as the maintenance of damaged pipes when mechanical interference happens during the service life of pipelines. [DOI: 10.1115/1.4040974]

1 Introduction

Mechanical interference such as collision and excavation plays an important role on the introduction of pipe structural damage [1–4]. Approximately, 23% of all the reported structural damage on pipelines in U.S. in the past 20 years is caused by mechanical interference [5]. Specifically, the mechanical interference may be scenarios such as dropped foreign objects [6], dragging anchors [7], excavations, operation of underwater fishing equipment [8,9], sinking vessels, and even mudslides on the sea bottom [2]. Damage, such as dents, metal loss, cracks, and combinations thereof, is therefore commonly found on metallic pipelines.

Such structural damage can be a serious threat to pipeline safety. The occurrence of damage on metallic pipes indicates a loss of performance. For small or medium damage, it is generally allowed on structures as long as it has satisfied some basic criteria. For instance, the maximum accepted dent depth in engineering practice should normally be less than 5%D according to DNV-OS-F101 [10]. Such damage may merely have an aesthetic effect such as the discoloring of the pipe coating. However, large

damage may bring severe consequences (so-called "significant incidents") in terms of local and/or global buckling, overall failure, and oil/gas leaking, etc. The number of significant incidents is between 41% and 53% of all the incidents according to the reported data [5] in the past years.

As one of the dominated loads encountered by a pipe, bending moment widely exists during its entire service life. For instance, pipes are exposed to a considerable large bending moment during a typical reeling installation: reeling-on, reeling-off, bending over the aligner, and bending through the straightening [11–15]. Another example is the large bending on spanned pipelines on the rough seabed [8], which appears when the contact between pipelines and the seabed is lost over an appreciable distance. Under this circumstance, the failure of pipelines with free span may be induced. As a result, the structure of damaged pipelines must be still able to withstand the anticipated bending load so that the service life of pipes can be effectively maintained.

In the last century, a considerable amount of experimental research has been carried out on damaged pipes. Most of the early studies [6,16–19] focused on the pipes with damage subjected to axial compression or external pressure or internal pressure. The considered D/t ratios of pipe specimens in these tests were normally between 30 and 90. Great efforts on theory and analytical solutions of damaged pipes are also made by researchers such as Ellinas [20], Bai [21], and Hauch [22].

In the beginning of the twenty-first century, the experimental research on bending capacity of intact metallic pipes began to thrive on. Gresnigt and Foeken [12] discussed the governing parameters such as geometrical deviations and material properties through four-point bending tests on pipes with D/t from 22 to 45. Vitali et al. [11] conducted pipe bending tests to investigate the local buckling and failure modes of thick pipes. Guarracino et al. [23] focused on the boundary effects due to a bending test. In the past few years, Hilberink [15] studied the bending capacity of an intact lined pipe. Es et al. [24] experimentally investigated the ultimate bending capacity of a spiral-welded steel pipe. Thirteen spiral-welded steel tubes with 42-in-diameter and D/t ranging from 65 to 120 were deployed for bending test.

Recently, researchers start to realize the importance of damage effect of pipes subjected to a bending moment. For instance, Levold et al. [13] carried out a bending test on a damaged pipe with $D/t = 26.5$, where corrosion damage in terms of gouge was artificially introduced by electrical discharge machining method. Cai et al. [25–28] numerically simulated the effects of damage on pipes after mechanical interference. Ghazijahani et al. [29] focused on the effect of a dent on the bending behavior of tubular members.

However, there is still a lack of systematic experiments on the residual bending strength of damaged metallic pipes suffering from mechanical interference. Therefore, the objective of the present research is to investigate the residual ultimate strength of metallic pipes with structural damage under a pure bending based on large-scale pipe tests. Large size damage is intentionally designed and properly produced in advance. It should be noted that the application of the test results to other full-scale pipes should be careful due to the possible scale effect. The entire experiments are carried out in the Structural Engineering Laboratory and Impact Laboratory, School of Transportation, Wuhan University of Technology, China. It should be also noted that, in spite of the fact that pipes are pressure vessel in reality, no internal pressure has been taken into account in the pipes during tests. Thus, no special design (such as end sealing) is introduced on the pipe ends.

The structure of this paper is arranged as follows: In Sec. 2 of this paper, a detailed description of the specimens and the test setups is given. The design of bending setup and damage-introduction methods are presented. In Sec. 3, the preliminary measurements of the pipe data are given. Geometrical parameters and material properties are presented. Corrections due to test methods are presented and discussed. Section 4 presents the results of bending capacity from the four-point bending tests. Comparison between test data and existing analytical solutions is given. The effect of each type of structural damage is discussed. In Sec. 5, further discussions on experimental errors are given. In the end, conclusions and suggestions are drawn.

2 Experimental Setup

In this section, the specimens and the test setups are presented. Specifically, outlines of the test design and configurations, materials, and measurement methods are described in detail. In addition, a description on how to properly introduce each type of structural damage on pipe specimens is given.

2.1 Outline of Tests and Specimens. To investigate the residual ultimate bending strength of damaged pipes, a test project on the large-scale steel pipe was completed. The major tests that have been completed in laboratory include the production of damage, material test, and four-point bending test.

The entire test project consists of 39 seamless specimens with nominal diameter-to-thickness ratio of 21.04, as shown in Table 1. The real diameter-to-thickness ratios of specimens vary from 20.41 to 23.75 due to the manufacturing deviation. Among all these completed specimens, four specimens are intact with no structural damage, whereas 35 are damaged with different types

Table 1 The principal dimension of specimens in four-point bending test

Parameters	Value
Full length of specimen (L) (mm)	2200
Half length under pure bending ($L1$) (mm)	400
Length of loading \ support strip ($L2 \backslash L4$) (mm)	100
Original bending length ($L3$) (mm)	300
Side length ($L5$) (mm)	200
Specimen type	Seamless (hot-rolled)
Specimen material	Q345B [30]
Nominal diameter	168.3 (mm)
Nominal thickness	8.0 (mm)

of structural damage. Among the damaged ones, there are eleven specimens with a dent introduced by quasi-static indentation, four specimens with a dent introduced by impact, five specimens with metal loss introduced by machining method, fourteen specimens with surface crack introduced by either machining or laser methods, another five specimens with combined dent, metal loss, and crack. The structural damage is introduced properly on the external surface of each specimen before strength test, locating on either its compression side or on its tensile side. The center of damage locates at the midspan of each specimen. All the specimens are acquired through the same production batch from the same provider at the same time, which makes sure that every specimen has a similar material property. Each specimen (L) is cut from an original pipe product with an overall length of 12 m in the structural laboratory.

An overview of the intact specimens without structural damage is shown in Table 5 in Appendix A, while an overview of the damaged specimens is shown in Tables 6–9 in Appendix A. For clarity reason, specimens are named and divided in different groups as follows: The intact specimens are put into the first group, naming from S1N1 to S1N4. The series number of specimens (S.N.) with a dent from quasi-static indentation is from S2N1 to S2N7, while specimens with impact induced dent damage are from S2N8 to S2N11 in the second group. The third group consists of specimens with metal loss, while the specimens with a single crack are put into the fourth group. Besides, the fifth group contains specimens with combined damage. Each damage is denoted by its length ($l_{(i)}$), width ($w_{(i)}$), depth ($d_{(i)}$), and rotation angle ($\theta_{(i)}$), as illustrated in Figs. 1 and 2, where i denotes the damage type, varying with different types by d, m, and c, respectively. The rotational angle of damage is defined as the angle between damage length and the longitudinal axis of specimen. The depth of dent is the depth between the lowest point of a dent in radial direction and the original pipe surface before deformation (see Fig. 1). It should be noted that Fig. 2 only contains the schema of dent parameters. The real measurement data are listed in Table 6. Furthermore, the structural damage is intentionally introduced at the center of each specimen, either on the compression side (C) or on the tensile side (T) of specimens. Before the introduction of structural damage, every intact specimen is visually inspected for a roughly integrity checking.

2.2 Outline of Material Test. The material property is one of the decisive factors to evaluate the ultimate strength of structures. The deployed pipe material is $Q345B$ [30], which is a typical material for transmission pipes with the specified minimum yield stress (σ_y) of 345 MPa. A tensile test has been deployed for measurement of the specific material properties. The dog-bone type of coupons is cut from both pipe longitudinal and hoop direction. The material coupons [31] cut from pipe longitudinal direction keep its original arc-shape, while the coupons cut from pipe hoop direction are flattened by a hydraulic machine with a low pressing speed (15 mm/s). Therefore, the hoop coupons may have a higher yield stress due to large plastic deformation for correction and the
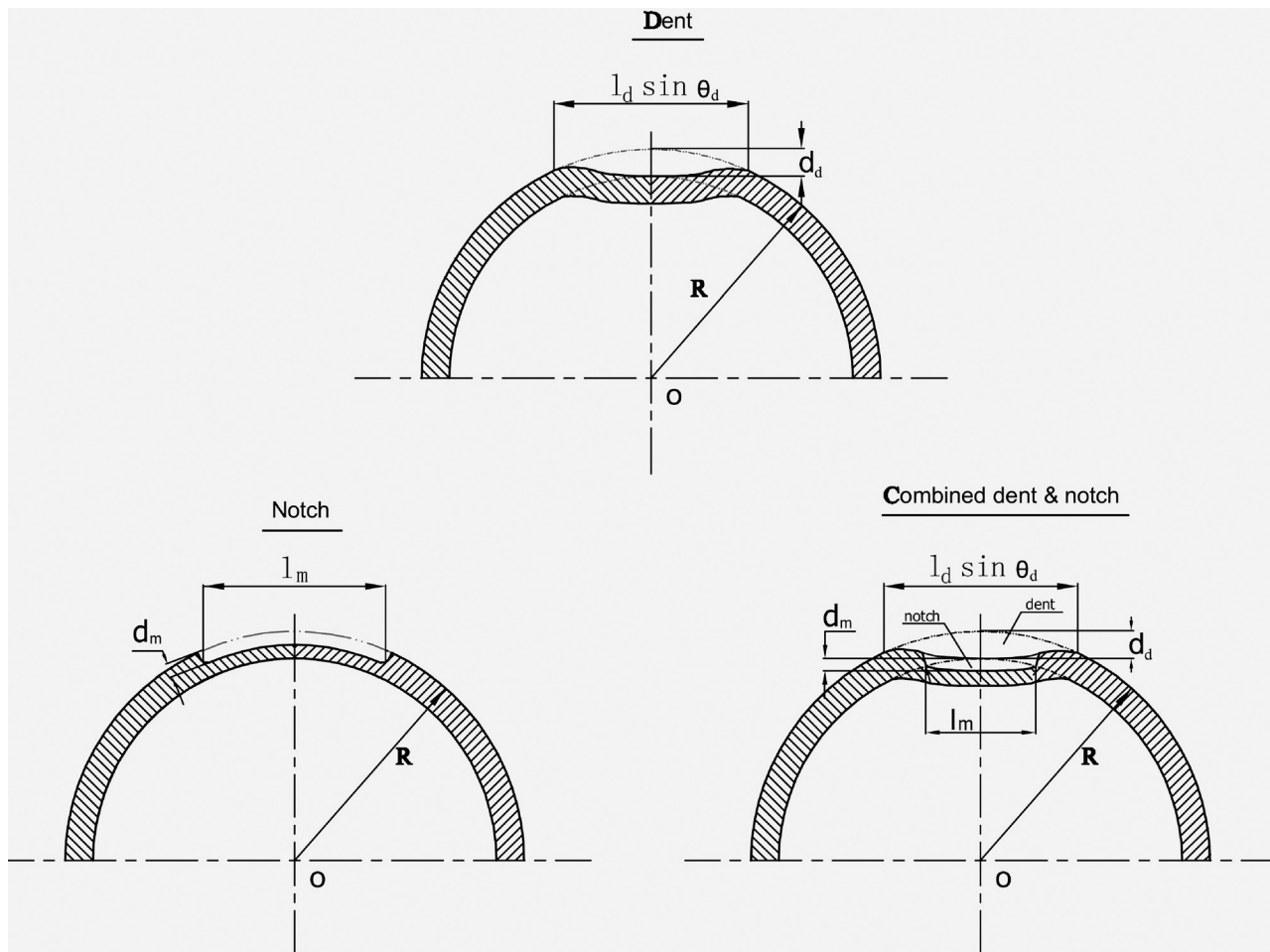
Fig. 1   Sketches of three different types of damage on the external surface of specimens (a dent, a notch, and combined dent and notch)

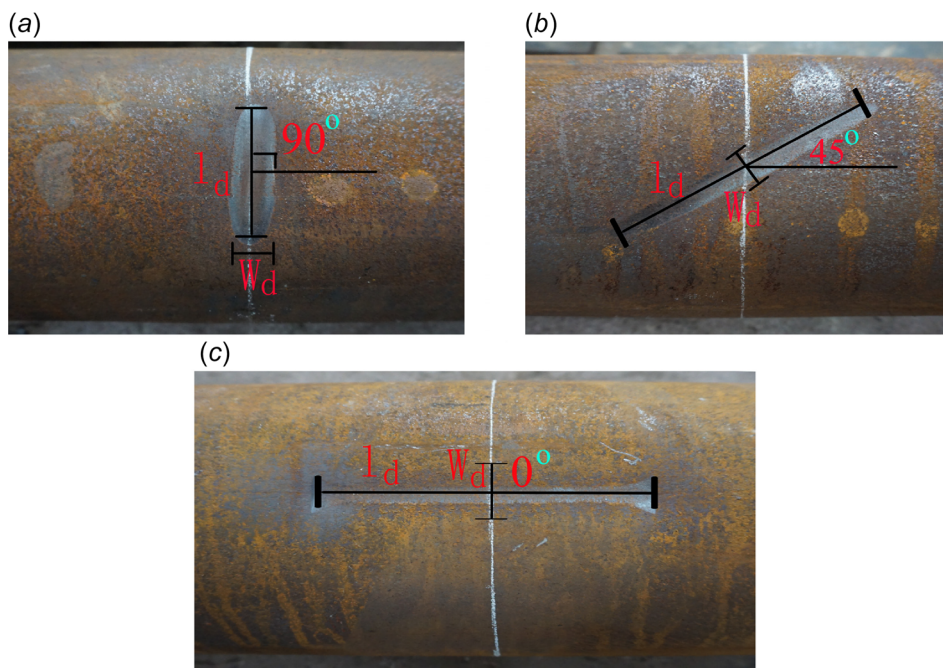**Fig. 2   A dent damage on the pipe surface with the schema of dent parameters in terms of dent width (w_d), length (l_d), and angle (θ_d): (a) the dent on S2N2 (90 deg), (b) the dent on S2N3 (45 deg), and (c) the dent on S2N4 (0 deg)**

(a)

(b)

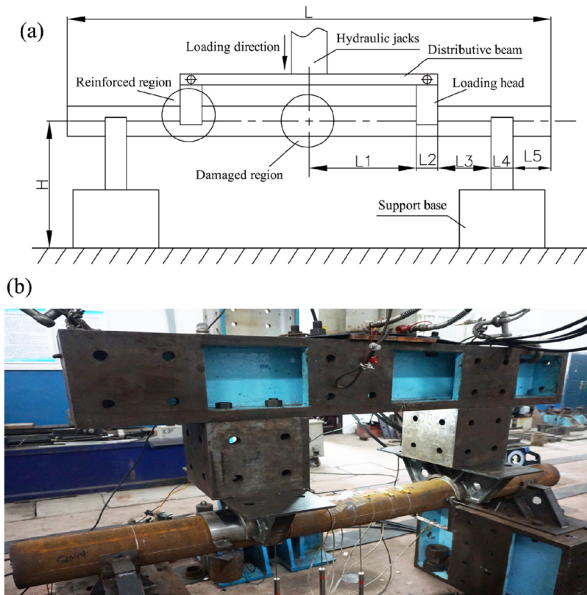**Fig. 3 The configuration of four-point bending structural test: (a) the design of bending test setup and (b) the real test setup in the laboratory**

Fig. 4 Scheme of bending data calculation in four-point bending test

strengthening effect. Detailed results are presented and discussed in Sec. 3.1. It should be noted that coupons are selected by random through the entire batch of pipes before the four-point bending test due to the laboratory limitation.

2.3 Four-Point Bending Test Setup. To determine bending capacity, the specimens are loaded in a four-point bending way. An overview of the test setup is shown in Fig. 3, while Table 1 lists the principal dimension of specimens. Boundary conditions have a strong effect on the magnitude of bending capacity and the distribution of stresses in a bending test. In this test, the design of boundary is to mimic the simply-supported boundary so that a pure bending can be accurately obtained. Hence, the translations of vertical and lateral direction have been fully constrained through loading heads and supports, whereas the axial translation is partially restrained through the friction force between the supports and the specimens. The support bases are fully fixed on the ground. The test setup has been designed to deliver the maximum force of 1200 kN through a distribution beam and hydraulic jacks. Therefore, sufficient loads can be guaranteed in order to collapse specimens. Four hydraulic jacks are fixed at the center of distributive beam so that a symmetrical loading pattern is introduced, having a force capacity of 300 kN and a stroke of 300 mm for each. The dead weight of the distributive beam is 1 ton, which is accounted for during bending moment calculation. A load-controlled strategy is deployed in the bending test. Specimens are loaded in fixed intervals in a consecutive way. During each loading interval, test situation is carefully inspected and extra data are recorded.

The configuration of pipe specimens is carefully designed. For instance, the overall length (L) is set to 2200 mm ($L/D = 13.07$), while the length under pure bending is designed to 800 mm ($L1/D = 4.75$). There are practical reasons for such design: According to the literature review [26] on existing bending test of intact pipes, a wide selection of overall length-to-diameter ratio of pipes is between 9 and 24. Considering the specific laboratory condition, therefore, a medium length ratio within this range is selected. Meanwhile, the minimum length of specimen under pure bending should be no less than four times of its outer diameter. In this way, the effect of loading head on pure bending will be effectively reduced. Reinforcements are also introduced so that local
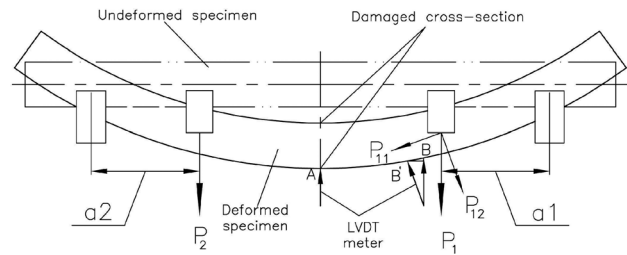
deformation and artificial failure of specimens can be avoided. A half-sleeve with a length of 200 mm and a thickness of 20 mm is therefore designed, as shown in Fig. 3. The internal diameter of the sleeve is the same as the outer diameter of the specimens so that a close contact has been reached. In this way, a test setup with symmetric boundaries and load conditions can be easily achieved. Extra heat treatment is used on the half-sleeve in order to increase its hardness.

In such a four-point bending test, the friction force between specimen and its supports and loading heads plays an important role. During loading, an equivalent axial compression force (P_{11}) has been introduced with the increase of the rotational angle of the specimen, as seen in Fig. 4. Under a certain range, the axial force is small and can be counterbalanced by friction force. As a matter of fact, the structure stays stable. The friction force helps to maintain such stability to some extent. However, when the rotational angle is sufficient large, such structural stability cannot be maintained by friction any more. As a consequence, a sudden sliding of specimen appears, which indicates that the boundary condition and force arm have been changed significantly. Hence, this phenomenon in four-point bending test is also used as the sign of test termination.

As described previously, some experimental errors, due to the test design and specimen dimensions, are unavoidable and should be corrected afterward. Strictly speaking, the real bending arm cannot keep constant during loading. Instead, it varies gradually with the increase of rotational angle of specimens. Such discrepancy is minor and can be neglected when the bending arm of specimen is much longer than the variation values.
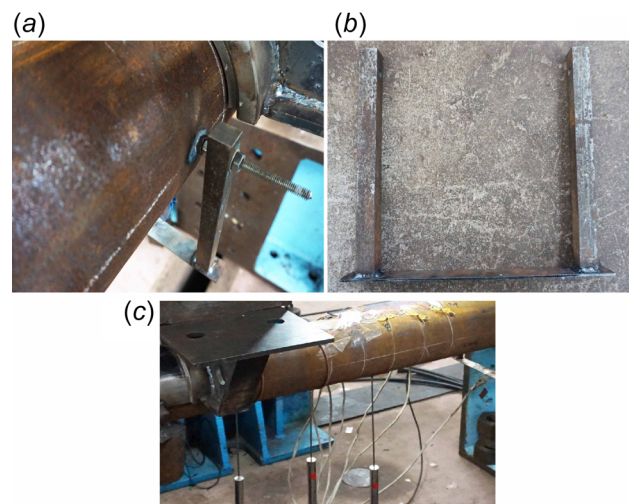
(a)   **(b)**

(c)

Fig. 5 Measurement tools in bending test: (a) configuration of the customized displacement meter on a specimen, (b) customized displacement meter, and (c) LVDT for measurement of vertical displacement and its configuration

However, extra measurement is needed in this test due to the relative short length of bending arm. The detailed correction method is described in Sec. 3.3.1. Another discrepancy needed to correct is the curvature due to the displacement measurement method through linear variable differential transformer (LVDT) in this paper. The detailed description of the correction method is presented in Sec. 3.3.2.

2.3.1 Measurement Methods. Important parameters are measured during bending tests. The loading forces (P_1 and P_2) are measured through a force transducer, as shown in Fig. 4. The horizontal ovalizations in critical cross section in the form of lateral displacement are measured by customized displacement meters, as seen in Figs. 5(a) and 5(b). Additionally, strains in terms of hoop and longitudinal components at critical locations are measured by strain gauges (range of ±3%). It should be noted that all the strain information are recorded discretely in this test. Therefore, these data are not listed in this paper.

The vertical displacements of specimen for curvature calculation are measured through LVDT meter with a measurement range of ±200 mm, as seen in Fig. 5(c). Critical locations such as 0D (central cross section), 05D (half pipe diameter offset from central cross section), one-dimensional (1D) (one pipe diameter offset from central cross section), and End-50 (50 mm offset from loading head) are selected for the deployment of LVDT meter. The selected points are located at the lowest location of each pipe cross section.

The customized displacement meter is made of two steel bars with large stiffness and a flexible flat steel with small stiffness, attaching to the neutral axis of the cross section of specimens during use. The strain gauges located at the center of flat steel are used to measure the variations of the bending strain. The lateral displacement can be then reflected based on such strain information. A calibration before measurement is necessary in order to obtain an accuracy result.

Equation (1) is deployed to calculate the bending curvature, where d_r is the relative vertical displacement between two measured points and l_{curv} is the corresponding longitudinal distance. Both local curvature (κ_1, κ_2) and global curvature (κ) are calculated based on the measured data. The local curvature is acquired between cross sections 0D and 1D or 1D and End-50 in some cases, while the global curvature is obtained between the cross sections 0D and End-50.

The global bending moment (M) is expressed by Eq. (2), where $a1$ and $a2$ are the real bending arms. However, it should be noted that such bending arms vary between 300 mm and 400 mm during the entire bending procedure, as discussed before. As a result, corrections are needed, as shown in Sec. 3.3

$$\kappa = 8d_r/l_{curv}^2 \qquad (1)$$

$$M_1 = P_1 \times a1$$
$$M_2 = P_2 \times a2 \qquad (2)$$
$$M_{ave}(M_{cr}) = (M_1 + M_2)/2$$

The strains in critical region are measured by a common type of electrical-resistance strain gauge with a measure range of ±3% in room temperature. Strain components in two directions (ε_{22} and ε_{11}) are measured. Workmanship is important for the accuracy of such measurement. Surface treatments of specimen are necessary such as polishing and cleaning. The gauge is carefully glued to the surface after treatments. Afterward, a mild pressure is executed in order to obtain a compact contact between the gauge and the specimen surface. In the end, silica gel is used for gauge protection.

Before the start of each bending test, the geometrical information of specimens including outer diameter and wall thickness is also measured. The outer diameter has been measured by a Vernier caliper in different pipe cross section, while the pipe thickness has been measured by an ultrasonic thickness gauge, as described in Sec. 3.2. Due to the limitation of laboratory conditions, the initial imperfection of specimen has not been measured. Instead, only visual checking is taken. However, this will not affect the further investigation of damaged pipes. According to the former research [7], initial imperfection only has insignificant effect on the bending capacity of pipes with low diameter-to-thickness ratio due to the large disturbance caused by bending moment.

2.4 The Production of Structural Damage. In order to introduce proper structural damage on specimens, different methods are deployed. The dent is produced by a customized indentor, while the metal loss in terms of notch is produced by mechanical machining method. The laser cutting technique is used to introduce a proper surface crack. For the combined damage, the introduction sequence of each single damage is important. Otherwise, the original size and shape of damage would be readily changed. In this test, the notch has been first fabricated, then a crack is produced at the notch tip, and a dent is introduced in the final step from indentation. A customized indentor with a bulge, which matches the notch shape, has been also fabricated to produce the dent for combined damage.

2.4.1 Dent. The dent on specimen surface is produced through two methods: quasi-static indentation and impact, as seen in Fig. 6. The aim is to study the dynamic effect produced by real mechanical interference. Different types of indentors are designed and fabricated to produce dents with varied shapes and rotational angles such as 90 deg, 45 deg, and 0 deg, as seen in Fig. 7. The indentor with bulge, as shown in Fig. 7(d), is deployed for the
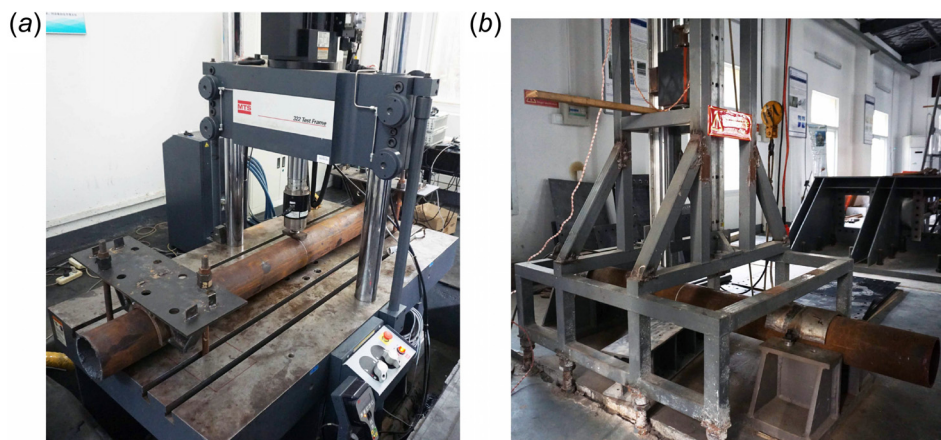

Fig. 6 Configuration of test setups for produce of a dent: (a) quasi-static indentation and (b) impact indentation
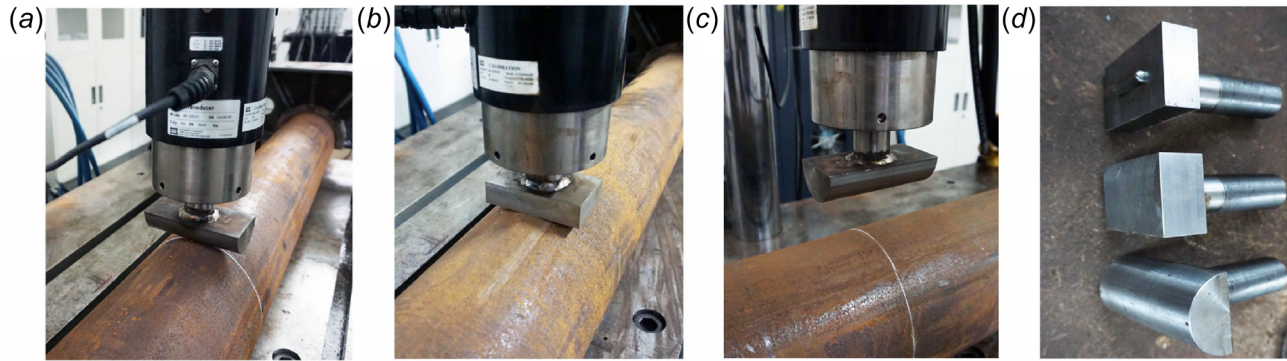
Fig. 7 The variation of indentor angle and shape in the indentation: (*a*) 90 deg, cylindrical shape, (*b*) 90 deg, rectangular shape, (*c*) 0 deg, cylindrical shape, and (*d*) different types of indentors
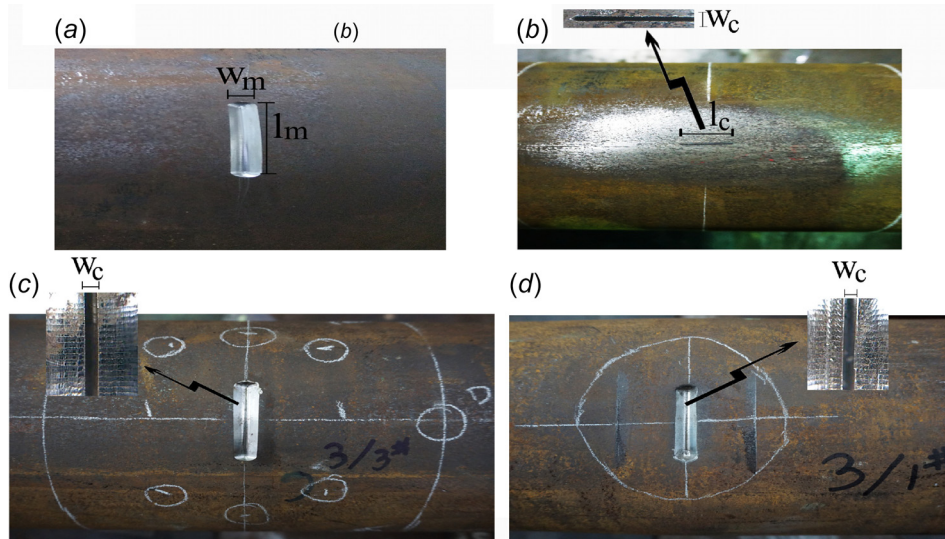

Fig. 8 Notch and crack damage on pipe surface: (*a*) single notch, (*b*) single crack (the crack can be seen from the zooming in area), (*c*) combined notch and crack (the crack can be seen from the zooming in area), and (*d*) combined dent, notch, and crack

introduction of a dent in combined damage. An example of such dent in combined damage is shown in Fig. 8(*d*). In this way, the existing damage can largely maintain its original size and shape after test. After the introduction of a dent, the size, location, and angle of damage are manually remeasured and documented for the following research (see Table 6).

The quasi-static indentation test is conducted on a MTS machine with a capacity of 25 ton (250 kN). Specimens lie on a solid platform with both ends fully fixed so that only local damage is introduced. The loading speed is set to 0.083 mm/s, which is slow enough to eliminate the possible dynamic effect during test. A displacement-controlled strategy has been deployed to produce the required dent with a designated depth.

For the impact test, a customized indentor with a weight of 54 kg is hoisted to an initial height of 2.45 m and then released in order to produce the structural damage, as seen in Fig. 6(*b*). The pipe ends are fixed, and the vertical displacement of the pipe central segment is constrained through a box girder. It should be noted that the bases cannot be fully fixed on the ground due to the limited laboratory condition, which dissipates the impact energy a little. Additionally, the repetitive impact due to bouncing back cannot be fully restrained, which leads to some scatters for the real geometrical size of the dent between the test and the original design. Despite the difference, the following bending tests of specimens will not be affected, since the damage dimensions are further measured before each strength test.

2.4.2 Metal Loss. The metal loss in the form of a notch is produced by the machining method. As shown in Fig. 8(*a*), the orientation of the notch in each specimen is constant with a rotational angle of 90 deg. A chamfer with radius of 1.5 mm is made at the notch tip in order to eliminate the random crack due to fabrication. Figures 8(*c*) and 8(*d*) show the combined damage which have been properly introduced. The notch depth is fabricated in parallel with the arc shape in hoop direction. However, the fabricated depth is not strictly constant due to the surface roughness of specimen. The notch ends are filleted into a steep slope.

2.4.3 Crack. As shown in Fig. 8(*b*), the surface crack has been properly introduced on the surface of the specimen. The detection of the variation of crack dimension is carried out through a portable crack detector. Two types of crack (shallow crack and deep crack) are fabricated in order to obtain the interaction effect between fracture and bending strength. The definition of the shallow crack in this paper is the crack with crack depth smaller than 1 mm and the crack width no less than 0.5 mm, which is fabricated by the machining method (S4N1–S4N6). With the increase of crack depth, this method is not suitable due to the limitation of the workmanship. Hence, the laser method has been deployed for a deep crack (a crack depth larger than 1 mm and a width less than 0.5 mm). Different crack locations and directions are used for each specimen, for instance, the tensile side and hoop direction in S4N1. There are two basic aims for the introduction

Table 2 Summary of material properties of coupons measured from the tensile test

S.N.	Yield stress (MPa)	Ultimate tensile stress (MPa)	Elongation (%)
L1	392	532	—
L2	388	548	—
L3	388	552	—
L4	400	583	22.6
L5	378	532	20.2
L6	380	563	21.6
L7	378	542	24.6
H1	404	506	—
H2	388	522	—
H3	402	545	16.0
H4	408	548	16.3

of such surface cracks. For the crack on the tensile side and in the hoop direction, the fracture failure in terms of the opening type (Mode I) is supposed to occur. In addition, in real impact scenarios, a crack along the pipe longitudinal direction is possible. Therefore, different types of crack are produced here.

The crack depth-to-half crack length ratios are 0.14, 0.42, 0.5, and 0.6 in the test, respectively. In addition, the surface of the cracked region is carefully ground in advance to eliminate the effect of surface roughness on crack depth. For the crack profile, it is impossible to make a specific shape such as the half-elliptical shape or the circular shape on structural surface under the current laboratory conditions. Therefore, a simple rectangular profile is made for all the cracks.

For combined damage, as shown in Figs. 8(c) and 8(d), the crack is introduced after the introduction of the notch. At the notch tip along its length, a tiny crack is cut by the machining method.

3 Results of Preliminary Measurements

In this section, the preliminary measurement data are presented. Specifically, results including material properties, wall thicknesses, and outer diameters are given. Correction methods for both bending arm and bending curvature are described and discussed. Meanwhile, statistical analyses on measured data such as the pipe wall thickness are carried out.

3.1 Material Properties From Tensile Test. A summary of the material properties of specimens in terms of yield stress (σ_y), ultimate tensile stress (σ_u), and elongation (ε_e) is presented in Table 2. Seven coupons (L1–L7) are cut from the longitudinal direction of specimens, while the other four coupons (H1–H4) are from the hoop direction of specimens. Yield stress of the specimens is obtained directly from the diagrams in Fig. 9. Normally, the value of 0.002 plastic strain is used to obtain the yield stress of coupons without yield plateau.

Figure 9 shows the stress–strain relationship of different coupons. A yield plateau occurs in coupons from the longitudinal direction, as seen in Fig. 9(a). However, it disappears in the coupons from the pipe hoop direction due to the flattening effect in coupon manufacture. A very similar stress–strain relationship in each coupon is obtained. It should be noted that the stress–strain relationship has not been accurately recorded after the postnecking of coupons due to the stress triaxiality in necking zone [32]. Equivalent fitting method [25] should be used to get the real relationship in this stage if necessary.

A slight anisotropy of pipe material has been introduced. For instance, the yield stresses of coupons in the hoop direction (H1–H4) are slightly larger than ($\sim3.68\%$) the ones (L1–L7) in the longitudinal direction. The ultimate tensile stresses of coupons in the hoop direction are slightly smaller than ($\sim3.64\%$) the ones in the longitudinal direction.

3.2 Wall Thickness and Outer Diameter. The pipe thickness (t) and outer diameter (D) of each specimen are manually measured before bending test, as seen in Tables 5–9. Followed by a strict surface preparation, i.e., polishing, surface cleaning and so on, the pipe thickness is measured by an ultrasonic thickness gauge. The general measured points are illustrated in Fig. 10. The pipe outer diameter is measured by a Vernier caliper for at least three times in each cross section to obtain an average value. The measured locations are generally the cross section in 0D, ±05D, and ±1D.

Additionally, an extra measurement is performed in several specimens in order to obtain the real distribution of both pipe wall thickness and diameter, providing an acceptance level of the
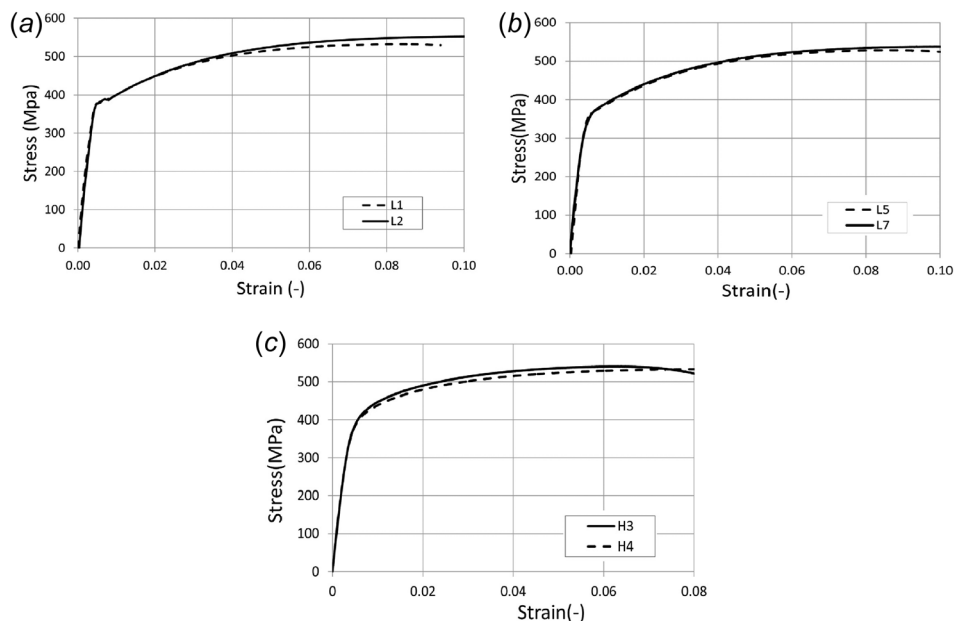

Fig. 9 The material stress–strain relationship from tensile tests: (a) coupons L1 and L2, (b) coupons L5 and L7, and (c) coupons H3 and H4
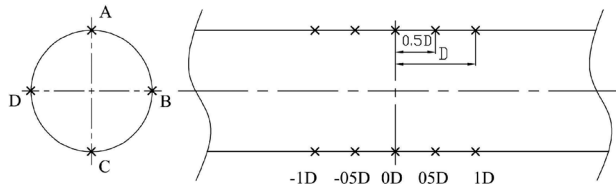
Fig. 10 The sketch of measuring points for thickness on a pipe surface

Table 3 Summary of average thickness and outer diameter of specimens in refined measurement

S.N.	Outer diameter (D) average (mm)	Thickness (t) average (mm)
1♯	168.38	8.21
S4N4	168.08	8.23
2♯	168.32	7.67
3♯	167.94	7.49

measured data. Such measurement of diameter is carried out in every cross section with an increment of 50 mm along the specimen axis. In each cross section, four points are selected for further thickness measurement. Therefore, there are at least 44 diameter data and 176 thickness data available in each specimen, which can be used for a reliable statistical analysis. Four specimens are used for such refined measurement, i.e. S4N4 and three other specimens (They are not included in the database of this paper, categorizing as 1♯, 2♯, and 3♯). It is expected that these data may reflect the accuracy and variation tendency of the pipe population (all specimens in this paper) in this test.

Assuming a normal distribution of measured data, the variation ranges of pipe diameter and thickness with a 95% confidence interval are presented in Fig. 11 (the mean value and standard deviation calculated from the finite coupons can be used as the true parameters). The average values from the specimens are summarized in Table 3. Results show that the spread of the wall thickness and the outer diameter within each specimen is small, whereas the variation of mean thickness is relative large between different specimens. For instance, the mean thickness of 3♯ is 7.49 mm, whereas the thickness of 1♯ is 8.25 mm. Another real distribution of measured data along the pipe axis is presented in
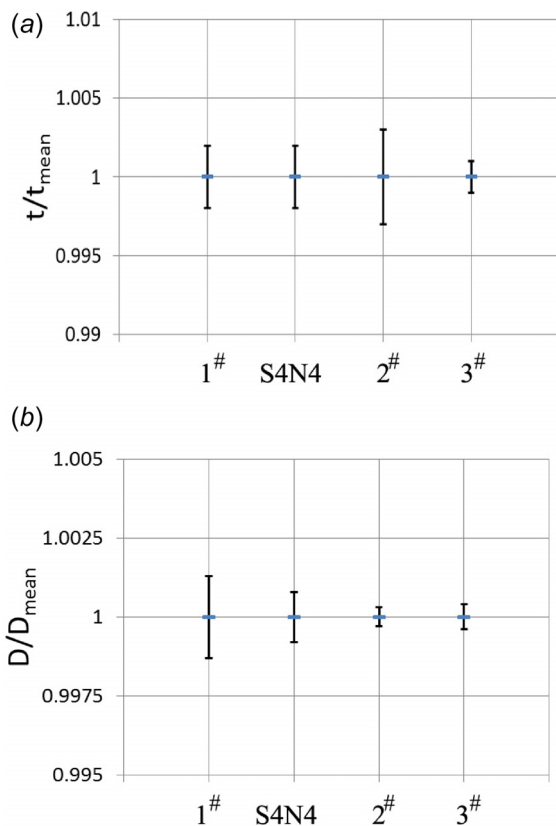
Fig. 12, where line 1 and line 2 are two respective parallel lines on the specimen surface.

3.3 Correction of Bending Arm and Curvature. As described in Sec. 2.3, corrections for both bending arm and curvature are needed in order to obtain a reasonable test result. Therefore, extra data are measured and presented in this section.

3.3.1 Bending Arm. The real bending arm cannot keep constant during loading due to the design of test setup, decreasing with the increase of bending angle. Theoretically, it varies from full bending length 400 mm to the original bending length 300 mm (L3) due to the variation of the true contact region between loading heads and specimen, as seen in Fig. 4.

In order to trace the relationship between true bending arm and loading time, extra measurements are added for each group of specimens. The correction procedure is listed as follows: At the end of each loading interval of a bending test, extra data including the bending arm and the corresponding loading time are recorded simultaneously. Provided that the variation of bending arm within each loading interval is uniform, the relationship is then fitted in terms of a polynomial diagram, as shown in Fig. 13. Therefore, the real bending moment can be corrected through such relationship.

3.3.2 Bending Curvature. As will be discussed in Sec. 5, the measurement method through LVDT provides an overestimation

Fig. 11 The 95% confidence interval of wall thickness and outer diameter of specimens: (a) wall thickness and (b) outer diameter
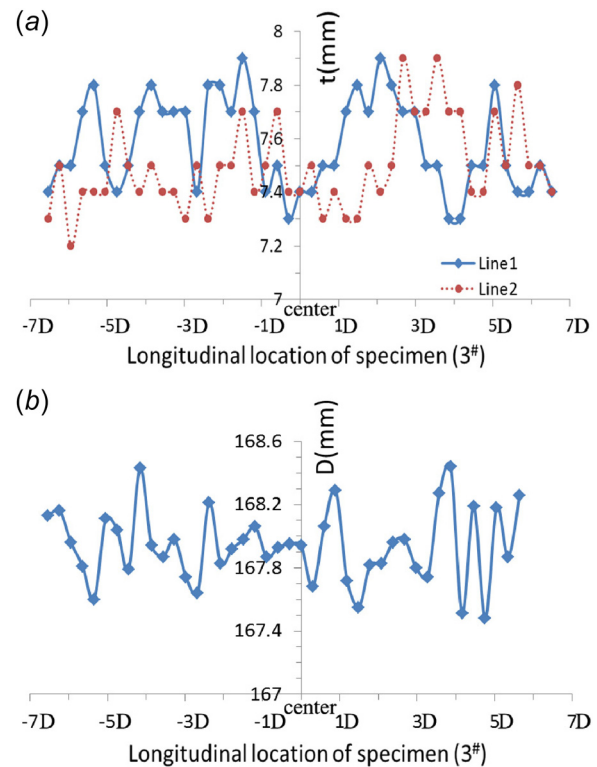

Fig. 12 The variations of pipe thickness and outer diameter on measured points along the pipe longitudinal direction: (a) wall thickness and (b) outer diameter
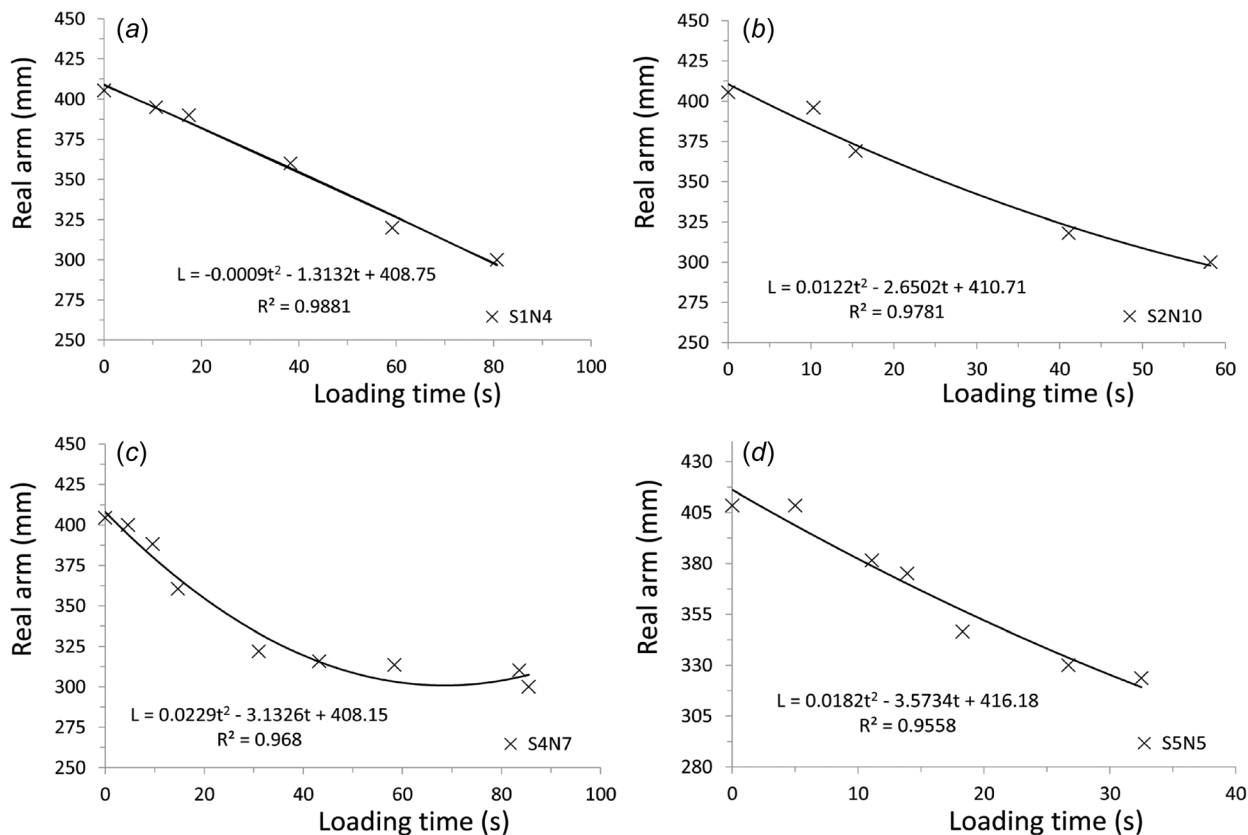
Fig. 13 The variation relationship between bending arm and loading time: (a) specimen S1N4, (b) specimen S2N10, (c) specimen S4N4, and (d) specimen S5N5

of specimen's curvature. Therefore, extra measurements are used to correct such experimental error.

It is easily derived that the curvature of a long beam during bending can be also written as Eq. (3), which is the function of the tangential angle (θ) of a given arc and the chord length of the arc (l_{curve}). Therefore, the tangential angle is measured manually at the end of each loading interval through a magnetic angle meter with dual scale and an accuracy of ± 1 deg. The corresponding curvature can be then calculated based on Eq. (3). After a careful comparison of curvature between the two mentioned methods, a correction coefficient is proposed for the curvature of each group of specimen, as shown in Table 4. By using this coefficient, a reasonable final curvature value is obtained

$$\kappa = \frac{2\sin(\theta)}{l_{curve}} \qquad (3)$$

4 Results of Four-Point Bending Tests

In this section, results in terms of structural failure mode, bending moment–curvature diagram, strength capacity, and critical

Table 4 Correction coefficients of curvature

| Series | ξ | | Series | ξ | |
	C^a	T^b		C	T
S1	1.645	—	S2	1.445	1.645
S3	1.445	1.645	S4	1.645	1.645
S5	—	1.645	—	—	—

[a]C denotes the specimen with damage on its compression side, the same in the following tables.
[b]T denotes the specimen with damage on its tensile side, the same in the following tables.

curvature are presented and discussed. The damage effect is presented and discussed through comparison. It should be noted that the series number of each specimen in this paper has been renumbered, for instance, the mark on the specimen S4N13 in Fig. 14(d). Hence, the numbers marked on some specimens do not necessarily match with the real series numbers in this paper.

4.1 Reference Values. For the bending moment–curvature diagrams in this paper, the bending is normalized by the plastic bending moment M_y, as seen in Eq. (4), while the curvature κ is normalized by the curvature-like expression $\kappa_0 = t/4R^2$. For the residual ultimate strength of damaged specimens, results from the average value of intact specimens are used for reference values. The reduction ratio of pipe ultimate strength can be written as $1 - M_{cr}/M_{intact}$.

$$M_y = 4R^2 t \sigma_y \qquad (4)$$

4.2 Structural Failure Modes. For pipes with low diameter-to-thickness ratio subjected to bending, they fail as a result of the increase of structural deformation in the form of ovalization in pipe cross section. Under a certain extent, such ovalization can be counterbalanced by the material yielding and further material hardening so that the structure stays stable. When the ovalization cannot be compensated for, the structure reaches its bending capacity with the largest ovalization in a specific pipe cross section. Hence, the structure fails with a certain failure mode.

The failure modes of different types of specimens are presented in Figs. 14 and 15. It is observed that an outward bulge is first formed on the compression side of intact specimen (S1N4) at the position of 25 mm away from the loading edge. With the increase of loading, a recession region is then fashioned in the adjacent surface of the outward bulge. Due to the lack of artificial damage, it
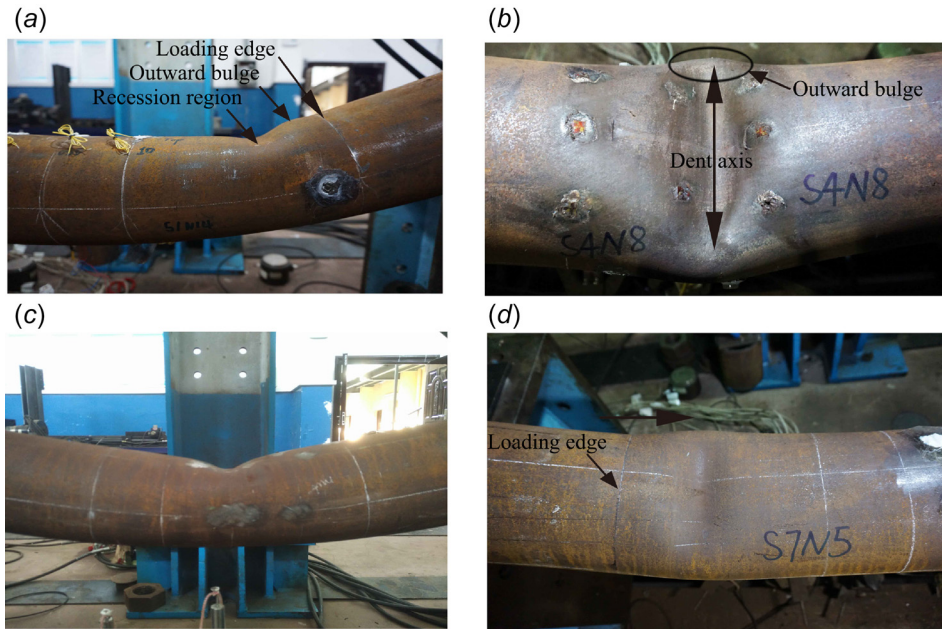
Fig. 14 The failure modes of specimens with damage on the compression side: (*a*) intact specimen (S1N4), (*b*) dented specimen (S2N4), (*c*) specimen with metal loss (S3N1), and (*d*) specimen with single crack (S4N13)
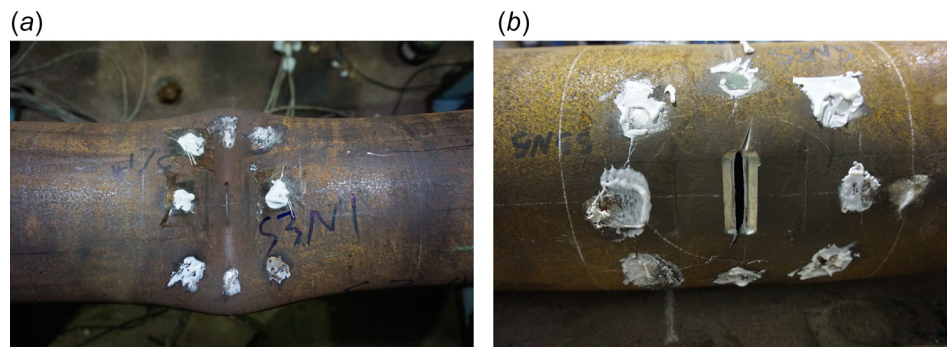

Fig. 15 The failure modes of specimens with combined damage: (*a*) specimen with combined damage on the compression side (S5N1) and (*b*) specimen with combined damage on the tensile side (S5N5)

is reasonable that the failure of intact specimen will initiate in the locations with structural discontinuity (reinforced sleeve, loading head, etc.).

The failure mode in dented specimen is different with the intact one. As seen from specimen S2N4 in Fig. 14(*b*), an inward, depressed region is rapidly developed in the dented area. Two outward bulges are then fashioned in the transverse direction of pipe. The dent angle, which is along the pipe axis, has not changed such failure tendency. For a dent on the tensile side (S2N7), a recovery of the existing dent occurs first, and then it fails in the same mode as intact specimen. Compared with a dent on the compression side, a similar failure pattern has been also observed on the specimen with metal loss (Fig. 14(*c*)) and on the specimen with combined damage (Fig. 15(*a*)) on their compression sides.

The fracture failure has been induced at a low loading force on specimen (as seen from S5N5 in Fig. 15(*b*)) with combined notch and crack on its tensile side. The propagation direction of fracture is about 45 deg along the notch axis. However, for specimens with a single crack either on the compression side or on the tensile side, no fracture failure has been observed. Instead, the same failure mode as intact specimen occurs, as seen in Fig. 14(*d*). The phenomenon will be further discussed in Sec. 5.

4.3 Moment–Curvature Diagrams. The bending moment–curvature diagram is one of the most important features of the strength of pipelines, which can reveal the variations of structural behavior in an explicit way. The calculation methods of bending moment and curvature have been described in Sec. 2.3.1. However, only the so called "global curvature (κ)" is presented due to the large discrepancy introduced by measurement method for the local curvatures. Further discussions are presented in Sec. 5.

The typical moment–curvature diagrams of both intact specimens and damaged specimens are presented in Figs. 21–27. It is observed from Fig. 21 (in Appendix B) that the diagrams in the listed four intact specimens have a very similar variation tendency. The intact specimens have a gradual and stable failure procedure due to the small diameter-to-thickness ratios. The vibration on the curve of case S1N1 is due to the external disturbance of data acquisition device during loading process. The occurrence of structural damage on the compression side of structures accelerates the failure due to the rapid localization of the damaged region, as seen from the diagrams for dented specimens in Fig. 22 and the notched specimens in Fig. 24. Detailed discussions of damage effect will be presented in Sec. 4.5.
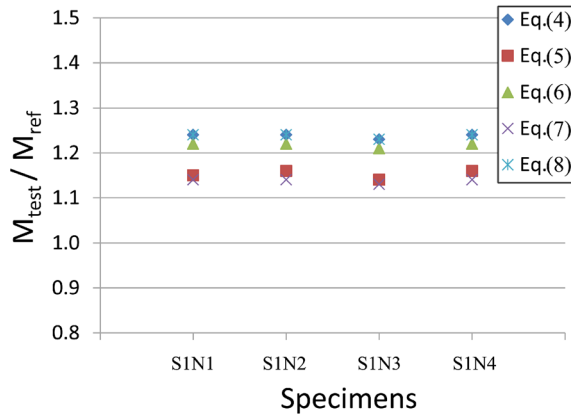
Fig. 16 Comparison of ultimate bending strength between intact specimens and existing analytical solutions

4.4 Comparison Results Between Test and Analytical Solutions. In this section, the comparison between experiments and existing analytical and/or empirical solutions on intact metallic pipes are carried out. The aim is to verify the accuracy of the test results. Due to the lack of formulas in damaged pipes, such comparisons are only for specimens without damage (S1N1–S1N4).

Figure 16 shows the comparison results of the normalized ultimate bending strength (M_{ref} is from the analytical formulas)

between intact specimens and analytical formulas. These formulas are listed in Eq. (5) [33], Eq. (6) [22], Eq. (7) [29], and Eq. (8) [34] from former researchers. Plastic bending moment is M_y in Eq. (4). The outer diameter D and outer radius R of pipe are used in these formulas.

From the engineering point of view, comparison results show a satisfying match between intact specimens and the analytical formulas. As expected, all formulas provide a conservative prediction for test specimens. The minimum discrepancy of ultimate bending moment between test and formulas is 13.75% from Eq. (7), while the maximum one is 23.75% from Eq. (8). The results are quite consistent in spite of the uncertainties such as the test methods [29]. In the following sections, damage effect will be analyzed through the comparison with the results from these intact specimens

$$M_{u2} = 3\sigma_u t R^2 \tag{5}$$

$$M_{u3} = \left(1.05 - 0.0015\frac{D}{t}\right)\sigma_y D^2 t \tag{6}$$

$$M_{u4} = 1.13 M_y e^{-X}$$
$$\text{Where } X = \sigma_y D/Et \tag{7}$$

$$M_{u5} = \frac{4}{3}\sigma_y\left(\left(R + \frac{t}{2}\right)^3 - \left(R - \frac{t}{2}\right)^3\right) \tag{8}$$
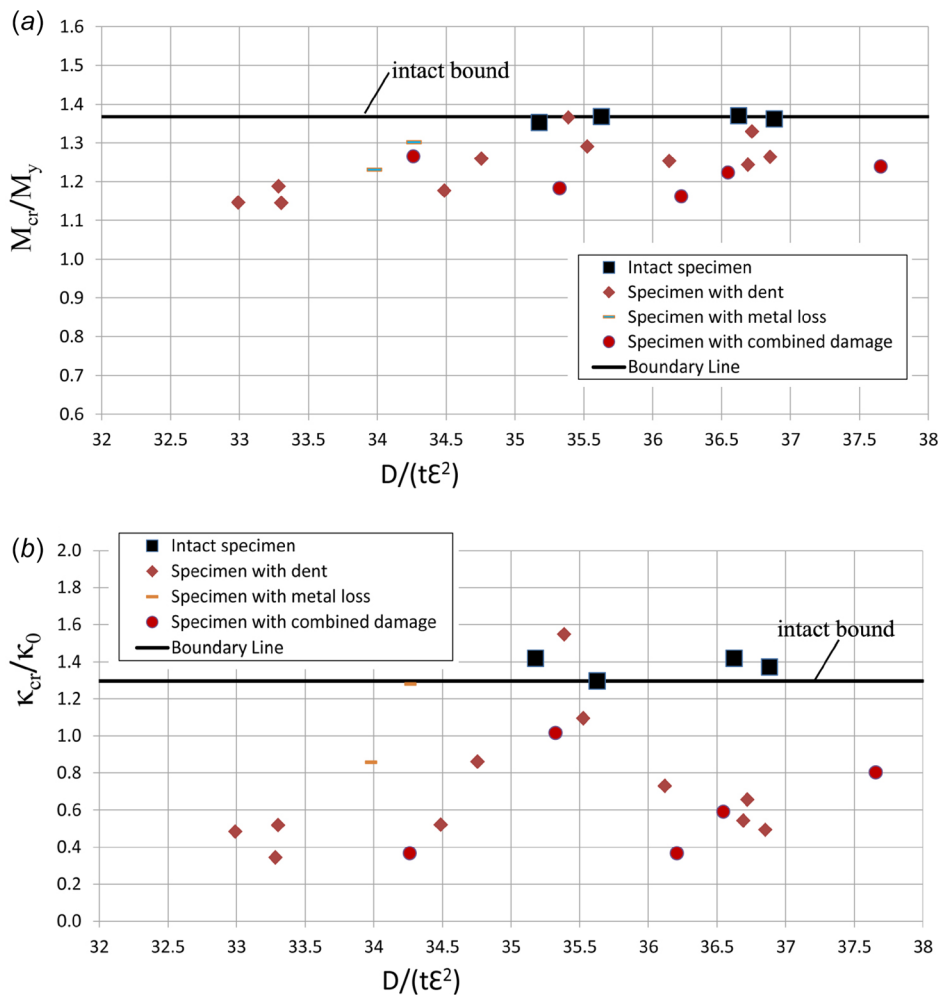

Fig. 17 The relationship between bending features in terms of M_{cr} and κ_{cr} and pipe slenderness: (a) normalized bending capacity (M_{cr}/M_y) and (b) normalized critical curvature (κ_{cr}/κ_0)
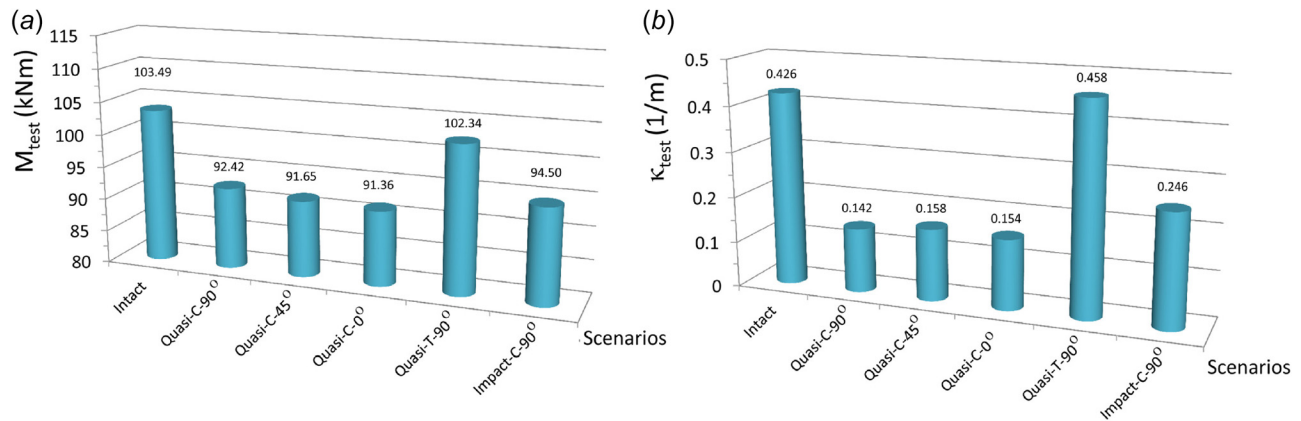
Fig. 18 Dent effect on ultimate strength of specimen in different scenarios: (*a*) ultimate bending moment and (*b*) critical curvature

4.5 Analysis of Structural Damage. In order to identify the effect of each structural damage, a detailed comparison is carried out in this section. Results in terms of the residual ultimate bending moment, the critical curvature, and the structural stable range are compared. Tables 5–9 list all the relevant results from the specimens.

A general comparison of bending features in terms of M_{cr} and κ_{cr} is shown in Fig. 17. The horizontal axis is the cross-sectional slenderness ($D/(t\varepsilon^2)$) of pipes, expressing as the function of the geometric slenderness (D/t) and material's yield stress, where ε^2 is equal to $235/\sigma_y$ based on rule [35]. It should be noted that results from cracked specimen are intentionally removed due to their abnormal large values. Discussions are conducted in Sec. 5. A boundary line (using the lowest value among the intact specimens) is also produced in order to have an explicit comparison. In addition, the surface strain ($\varepsilon = \kappa D/2$) is used in order to compare the stable range before collapse of each specimen. For instance, the average stable strain range for intact specimens is between 1.02% and 3.91%, as seen in Fig. 21.

Results show that structural damage, including a dent, a notch, and combined damage on the compression side of the pipes, has a significant effect on their bending strength. For the damage on the tensile side of specimens, ultimate strength mainly depends on the appearing of fracture failure. For the case with a dent on its tensile side (S2N7), only a slight reduction of bending capacity occurs. However, a larger critical curvature is produced due to the recovery of the existing dent shape, as mentioned in Sec. 4.2.

4.5.1 The Effect of Dent. A more specific comparison is presented in this section to obtain the effect of a dent. As seen in Fig. 18, a comparison of the dent effect on residual strength under different scenarios is carried out. Five different scenarios are used, categorized according to the introduce method of a dent and the dent rotational angle. The average values of specimens with similar dent depth are used as a single category, in spite of the existing discrepancies between each specimen. For instance, the "Quasi-C-90" scenario consists of specimens S2N1, S2N2, S2N5, and S2N6 with the same dent depth (10.3 mm), and with the dent on the compression side in pipe hoop direction produced by the quasi-static indentation. The "Impact-C-90" consists of specimens from S2N8 to S2N11 with a similar dent depth, and with the dent on the compression side in pipe hoop direction produced by the impact indentation (Fig. 6(*b*)). It should be noted that quantification of damage effect cannot be done due to the limited number of specimens in the test. Other research is needed, as seen in the published papers by the authors [36,37].

Results from Fig. 18 show that a dent on the compression side has a significant negative effect on pipe strength. For instance, the largest reduction ratio of ultimate bending has reached 11.72%,

while the largest reduction of critical curvature is 66.67%. A rapid failure occurs due to such dent, as seen in Fig. 22.

Compared to the scenarios with a dent introduced by quasistatic indentation, the impact effect has not produced obvious difference. The reduction ratio of ultimate bending is 8.68%, while the reduction ratio of critical curvature is 42.25%. In addition, there is a similar negative effect of dent with different rotational angle, as seen from scenarios "Quasi-C-90", "Quasi-C-45," and "Quasi-C-0". Therefore, a further quantification of both dent angle and impact effect is still needed to be done.

It is observed that there is only a slight effect of ultimate strength for the specimen (S2N7) with a dent on its tensile side. For instance, the reduction ratio of ultimate bending is 1.11%. Due to the recovery of a dent on the tensile side, as described in Sec. 4.2, the critical curvature has increased a little (7.5%). However, the bending moment is, at any situation, reduced due to the occurrence of the dent.

For the stable range of strain before specimen failure, it has been largely reduced for the specimens with a dent on the compression side (from 0.54% to 1.67%), as calculated from Fig. 22, whereas it is pretty close to the intact specimens for the specimens with a dent on the tensile side (from 1.74% to 5.08%).

4.5.2 The Effect of Metal Loss. The metal loss in terms of a notch has been properly introduced on pipe specimens. All the notches are put at the center of specimen with the angle of 90 deg. The notch on specimens including S3N1, S3N2, and S3N3 is on the compression side, while the notch on specimens S3N4 and S3N5 is on the tensile side. Exceptions happened on specimens S3N1, S3N2, and S3N5 due to the pre-failure of loading region caused by the insufficient reinforcement. Their failures initiate in the region close to the loading head instead of the damaged region. However, all the moment–curvature diagrams of notched specimens are still presented as a comparison, as seen in Fig. 24.

For clarity reason, the effects of both notch and combined damage are presented in Fig. 19. Different scenarios are also used for comparison. "Notch-T" means the scenario of a notch putting on the tensile side of specimen. "Dt & Nth & Crk-C" means the scenario of the combined dent, notch, and crack damage on the compression side of a specimen. A significant negative effect has been introduced for a notch on the compression side. For instance, the reduction ratio of bending is 10.24%, while the reduction ratio of critical curvature is 37.09%.

Fracture failure appears on the specimen (S3N4) with notch on its tensile side. Its bending capacity majorly depends on when and where the fracture starts to propagate. It is observed that in this case, fracture starts to initiate and propagate at the bending moment of 100 kNm and the critical curvature of 0.393 1/m, as shown in Fig. 19. In addition, such fracture failure has not changed the variation of moment–curvature diagram, as shown in
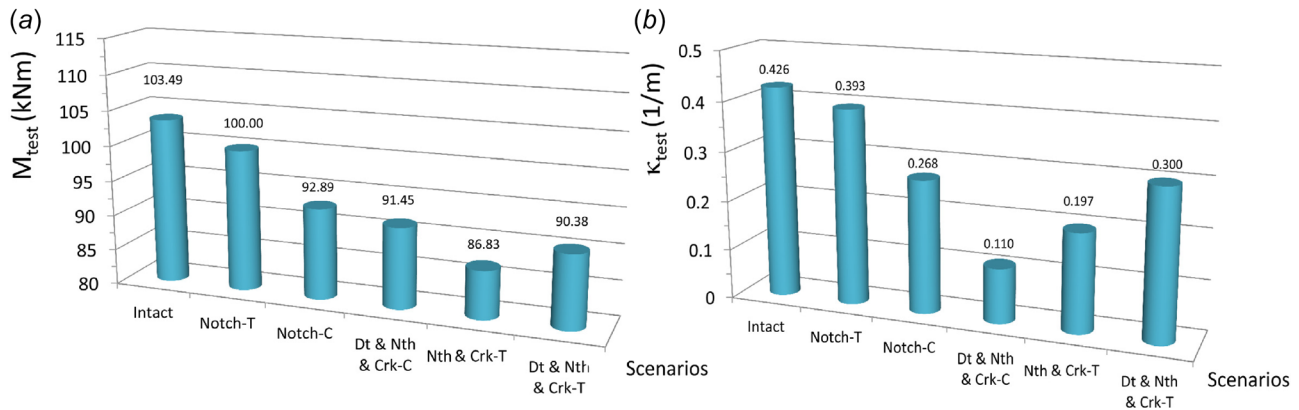
Fig. 19 Notch and combined damage effects on ultimate strength of specimens in different scenarios: (a) ultimate bending moment and (b) critical curvature
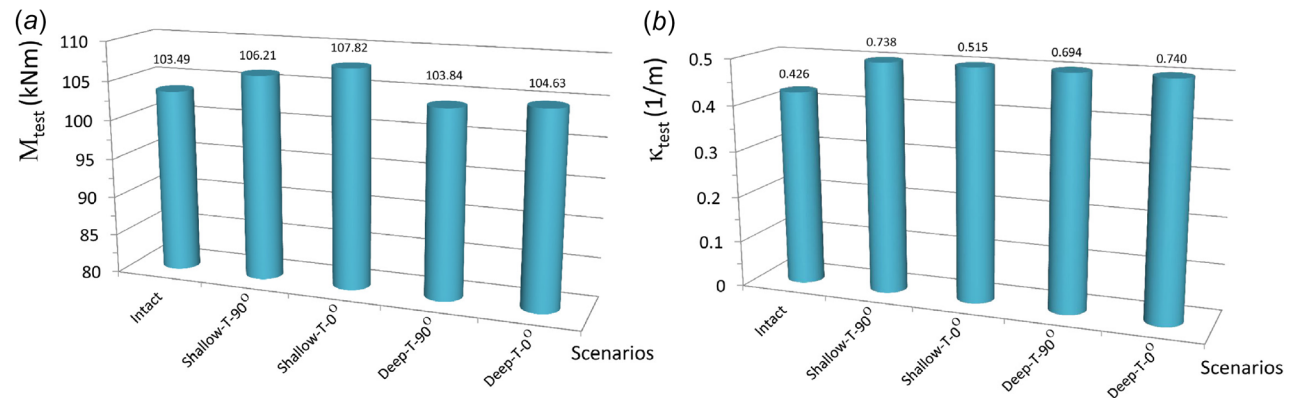

Fig. 20 Crack effect on ultimate strength of specimens in different scenarios: (a) ultimate bending moment and (b) critical curvature

Fig. 24(*d*). The stable range of strain has been significantly reduced (from 0.54% to 0.93% for notch on the compression side), as seen in Fig. 24.

4.5.3 The Effect of Crack. In order to investigate the crack effect, a single crack has been introduced to the pipe surface. The single crack in each specimen is set at different locations and directions. For instance, specimen S4N1 has a crack on its tensile side and in the hoop direction, while specimen S4N4 has a crack on its compression side and in the longitudinal direction. The so-called shallow crack in Fig. 25 in this paper is a crack with a depth less than 1 mm, while the deep crack in Fig. 26 is a crack with a depth larger than 1 mm.

Figure 20 shows the comparison results of crack effect on pipe bending strength. "Shallow-T-90" scenario means the specimen with a shallow crack on its tensile side and in the hoop direction. It is observed that there is an occurrence of positive effect for all the specimens with a crack on the tensile side, which obviously violates the common sense. For instance, an increase of 4.18% in ultimate bending moment at a larger curvature (0.515 1/m) occurs in the scenario of "Shallow-T-0 deg." No fracture has been initiated, and the bending moment–curvature diagrams in all these cracked specimens are very close to the intact specimens, as shown in Figs. 25 and 26.

Accounting for the laser cutting method to produce crack in this test, it is possible that a strengthened region in specimen has been produced due to the heat affected zone (HAZ). Noticed in the research of Miraoui et al. [38], the HAZ generated by the laser cutting introduces a high hardness to a maximum depth of 0.5 mm. Hence, such strengthened region shields the initiation and propagation of the crack and produces a higher ultimate strength in these specimens. However, it is impossible to quantify its effect due to lack of data, which would be a part of future research. Discussions will be further made in Sec. 5.

4.5.4 The Effect of Combined Damage. The combined damage is more prone to appear on the structural surface in reality. Two types of combined damage are therefore introduced and presented here. One is the combination of metal loss and crack, the other is the combination of metal loss, dent, and crack. As shown in Fig. 19, three different scenarios of combined damage are compared. Dt & Nth & Crk-C means the scenario of combined dent, notch, and crack on the compression side of specimen.

Results show that the combined damage has the most severe effect on pipe ultimate strength. For combined damage on the compression side, the reduction ratio of ultimate bending moment is 11.63%, while the reduction ratio of critical curvature is 74.18%. The results indicate that a rapid failure occurs at the lowest curvature. Figs. 27(*a*) and 27(*b*) also demonstrate this phenomenon according to the variation of bending moment–curvature diagram. In addition, for combined damage on the tensile side, fracture failure in terms of Mode I has occurred in a very early time during loading. As shown in the combined notch and crack scenario in Fig. 19, the initiation and propagation of crack happened at the bending moment of 86.83 kNm and the curvature of 0.197 1/m.

5 Discussions

In this section, the possible causes for the introduction of experimental errors in this test are discussed in order to have a better understanding of the real physical mechanism of pipe strength.

As mentioned in Sec. 4.5.3, a strengthening phenomenon has been observed for the specimens with a single crack. The major cause of such abnormal phenomenon is the strengthened region induced by laser cutting technique. The laser cutting technique was used for the introduction of a surface crack. Compared to conventional cutting, it has more advantages such as accurate cutting, noncontact processing, and short time of processing. Therefore, the designated crack dimensions are properly fabricated in this test. However, the HAZ generated by this technique may lead to undesirable effects on the structure. The HAZ is the zone of the base material, which has not melted but whose microstructure and mechanical properties are affected by the heat generated during laser cutting. Hence, a much higher hardness of the material in the vicinity of the surface crack region is induced. As a consequence, the induced martensite around the crack creates a high-strengthen region, effectively strengthening the pipe structure and shielding the effect of crack. Further research is needed in order to quantify its effect so that the real interaction between fracture and ultimate strength could be revealed.

A shear force exists due to the use of loading heads in the four-point bending test. The strain distribution of the pure bending segment ($2L1$) has been affected as a consequence. Pre-failure of structure will be introduced in the region adjacent to the loading heads due to the change of such strain distribution. One of the methods to alleviate the effect is to extend the segment length of specimen under pure bending ($2L1$). Thus, the affected region of shear force will be restricted in a very limited area. In addition, a reinforcement in the loading region is necessary in order to avoid the pre-failure of specimens due to shear force. A special designed half-sleeve is used in this test. By using half-sleeve, its own stiffness should be carefully checked after each test in order to guarantee the accurate behavior of pipe behavior. For instance, exceptions appear on specimen S3N1, S3N2, and S3N5 due to the softening of the half-sleeve, as seen from Figs. 24(a), 24(b), and 24(e). The effect of damage has been shielded by the pre-failure of structure in the regions adjacent to the loading head.

The variation of the real bending arm in four-point bending test and its correction method may introduce experimental errors. With the gradually increased rotational angle of specimen during loading, the contact area between the loading heads and the specimen is decreasing. The real bending arms ($a1$ and $a2$) cannot stay constant any more, varying between 300 mm to 400 mm in this test. Therefore, a reasonable correction on the bending arm of each specimen is needed, as descried in Sec. 3.3. The assumption of uniform variation of bending arm within each loading interval has therefore introduced some experimental errors.

Another major cause is the measured method of the pipe curvature through LVDT displacement meter. The LVDT meter is used to measure the vertical displacement in specific points. The installation of LVDT meter is realized by the use of a glue and cotton, fashioning a so called "elastic-connection" between the specimen and the meter. The base of the meter is fixed to the ground. Such connections are supposed to be stable and can resist the variation of large deformation. The problem is that the displacement meter will incline inward and slide slightly (point B to B') due to such design, as seen in Fig. 4. Under this situation, the measured vertical displacement (point B' in Fig. 4) is larger than the true value. As a consequence, the calculated vertical displacement d_r becomes larger, which means an overestimation of the curvature in this test. Furthermore, the error induced by this method would be more significant with the decrease of the longitudinal span (l_{curv}), as expressed in Eq. (2). Therefore, only the so-called global curvature with a long span (l_{curv}) is finally adopted in this paper. In order to correct such effect, extra data such as rotational angles in each loading interval have been measured by a magnetic angle meter, as described in Sec. 3.3.

Other causes in this test may also induce discrepancies as well, such as the slightly coarse inner surface of specimens, which may affect the measurement accuracy of pipe thickness, the strengthening effect due to unloading, the accuracy of the material property

due to the stress triaxiality after coupon necking, and the restriction of ovalization by loading heads. As stated in the research from Guarracino et al. [23], the ovalization restriction of pipe specimen will introduce discrepancy in strain distribution.

6 Conclusions

This paper has conducted an extensive experimental investigation on the residual bending strength of seamless metallic pipes with different types of structural damage. The seamless specimens with a nominal diameter-to-thickness ratio of 21.04 are used. The structural damage is properly introduced. The damage effects are explored through comparisons. The conclusions of this paper are drawn as follows:

(1) Different failure modes have been observed in this test. Intact pipe failed on its compression side close to the loading head in the form of an outward bulge. For a pipe with damage (a dent, notch and combined dent and notch) on its compression side, structure failed rapidly in the form of an inward, depressed region in the damaged region. Additional outward bulges along the damage axis also occur.

(2) For a pipe with a dent on its tensile side, a recovery of the existing dent occurs first, and then it fails in the same mode as intact specimen. The fracture failure has been induced at a low loading force on pipe with combined notch and crack on its tensile side.

(3) The ultimate strength of the intact specimen has a satisfying agreement with the analytical formulas from former researchers.

(4) Structural damage includes a dent, a notch, and combined damage on the compression side of pipes has a significant effect on their bending strength. The ultimate strength of damaged pipes on the tensile side mainly depends on the appearing of fracture failure.

(5) A considerable reduction of bending strength is induced by a dent on the compression side of pipes, whereas only a light effect is observed for a dent on the tensile side due to damage recovery. The effects of impact and dent parameters such as rotational angle cannot be quantitatively obtained in this research. The relative angle between the dent direction and the applied loads should be considered. Further research is needed to be done.

(6) A considerable reduction of bending strength is induced by the metal loss on the compression side of pipes. Fracture failure dominates the pipe behavior when the metal loss is on its tensile side.

(7) The interaction effect between a single crack and the strength has been shielded by the strengthening effect of a heat affected region. A high hardness region is induced by the introduction of a crack through laser cutting technique.

(8) The combined damage has the most severe effect on pipe ultimate strength. The largest reduction ratio of bending capacity has reached 11.63%, while the reduction ratio of critical curvature is 74.18%. Further research is needed to quantify the effect of specific damage parameters in the combined damage.

The test data obtained in this experimental investigation can be applied to the future quantification of the damage effects on the bending capacity of seamless pipes with similar D/t ratios when mechanical interference happens during the service life of pipelines. The comparison results between different types of structural damage can provide an insight, and be used to facilitate the decision-making of engineers when they need to estimate the residual strength of damaged pipes. Great efforts are also put into the discussions of experimental errors in this paper, which will help other researchers to optimize their own test set-ups for residual strength investigation. Due to the limited number of specimens in this test, further studies on extensive damage dimensions and

different types of pipes are still needed in order to quantify the damage effect and to extend its application domain.

Acknowledgment

Funding Data

Nomenclature

a1(a2) = real bending arm (mm)
D = outer diameter of pipe (mm)
d_c = crack depth (mm)
d_d = dent depth (mm)
d_m = metal loss depth (mm)
d_r = relative vertical displacement between measured points (mm)
L = full length of specimen (mm)
l_c = crack length (mm)
l_d = dent length (mm)
l_m = metal loss length (mm)
l_{curv} = longitudinal span of measured points (mm)
L1 = half length of specimen under pure bending (mm)
L2(L4) = length of half-sleeve strip (mm)
L3 = original bending arm (mm)
L5 = side length of specimen (mm)
M_{cr} = residual ultimate bending moment (kNm)
M_y = plastic bending moment (kNm)
$M_1(M_2, M_{ave})$ = bending moment (kNm)
$P_1(P_2)$ = vertical force on specimen (kN)
$P_{11}(P_{22})$ = force component (kN)
R = outer radius of pipe (mm)
t = pipe thickness (mm)
w_c = crack width (mm)
w_d = dent width (mm)
w_m = metal loss width (mm)
ε_e = elongation of material
ε_{11} = strain component in pipe axial direction (MPa)
ε_{22} = strain component in pipe hoop direction (MPa)
κ = global curvature of specimen (1/m)
κ_0 = referential curvature of pipe (1/m)
κ_{cr} = critical curvature of pipe (1/m)
σ_u = ultimate tensile stress of material (MPa)
σ_y = material yield stress (MPa)

Appendix A: Tabular Summary of Test Results for Specimens Under Bending

This Appendix presents a tabular summary of each type of pipe specimens in terms of measured geometry, critical bending moment, and critical curvature.

Table 5   The overview of intact specimens (dimension unit: mm)

S.N.	D	t	D/t	M_{cr}[a] (kNm)	κ_{cr}[b] (1/m)
S1N1	168.09	7.90	21.28	104.37	0.422
S1N2	167.36	7.87	21.27	103.65	0.439
S1N3	167.55	7.92	21.16	103.21	0.441
S1N4	167.01	7.84	21.30	102.71	0.401

[a]M_{cr} denotes the bending capacity of specimen, the same in the following tables.
[b]κ_{cr} denotes the global curvature measured from test, the same in the following tables.

Table 6   The overview of specimens with dent damage (dimension unit: mm; angle unit: degree)

S.N.	D	t	D/t	Dent ($l_d \times w_d \times d_d$)	Dent angle	Location	M_{cr} (kNm)	κ_{cr} (1/m)
S2N1	169.21	8.25	20.51	$89 \times 68 \times 10.3$	90	C	92.57	0.154
S2N2	168.23	8.13	20.69	$100 \times 75 \times 10.3$	90	C	93.55	0.109
S2N3	169.38	7.90	21.44	$130 \times 60 \times 10.3$	45	C	91.65	0.158
S2N4	169.26	7.42	22.81	$150 \times 30 \times 10.3$	0	C	91.36	0.154
S2N5	168.74	8.15	20.70	$110 \times 85 \times 10.3$	90	C	90.97	0.164
S2N6	169.31	7.39	22.91	$80 \times 60 \times 10.3$	90	C	92.58	0.139
S2N7	168.52	7.66	22.00	$95 \times 60 \times 10.3$	90	T	102.34	0.458
S2N8	167.19	7.57	22.09	$43 \times 40 \times 10$	90	C	94.11	0.325
S2N9	168.54	7.80	21.61	$60 \times 40 \times 8$	90	C	95.96	0.260
S2N10	168.25	7.37	22.83	$60 \times 80 \times 9.6$	90	C	95.88	0.187
S2N11	168.42	7.50	22.46	$60 \times 40 \times 12$	90	C	92.03	0.211

Table 7   The overview of specimens with metal loss damage (dimension unit: mm; angle unit: degree)

S.N.	D	t	D/t	Notch ($l_m \times w_m \times d_m$)	Notch angle	Location	M_{cr} (kNm)	κ_{cr} (1/m)
S3N1	167.03	7.40	22.57	$44 \times 10 \times 3$	90	C	106.34	0.327
S3N2	167.31	7.54	22.19	$45 \times 10 \times 3$	90	C	95.10	0.412
S3N3	166.89	7.90	21.13	$45 \times 10 \times 3$	90	C	92.89	0.268
S3N4	168.30	7.90	21.30	$45 \times 10 \times 3$	90	T	100.00	0.393
S3N5	167.96	8.23	20.41	$45 \times 10 \times 3$	90	T	105.96	0.321

Table 8 The overview of specimens with crack damage (dimension unit: mm; angle unit: degree; damage Size: $l_c \times w_c \times d_c$)

S.N.	D	t	D/t	Crack	Angle	Location	M_{cr} (kNm)	κ_{cr} (1/m)
S4N1	167.01	7.10	23.52	$10 \times 0.5 \times 0.70$	90	T	107.76	0.691
S4N2	168.42	7.58	22.22	$10.5 \times 0.52 \times 0.75$	90	T	104.65	0.785
S4N3	167.70	7.30	22.97	$10.5 \times 0.54 \times 0.70$	90	C	100.34	0.259
S4N4	168.08	8.23	20.42	$10.5 \times 0.5 \times 0.70$	0	C	116.29	0.219
S4N5	167.80	8.08	20.77	$10.5 \times 0.5 \times 0.70$	0	T	106.09	0.698
S4N6	168.19	8.03	20.95	$10.5 \times 0.5 \times 0.70$	0	T	109.55	0.332
S4N7	168.3	7.50	22.44	$10.00 \times 0.35 \times 2.10$	90	T	108.60	0.729
S4N8	168.20	7.66	21.96	$10.00 \times 0.22 \times 2.50$	90	T	100.69	0.717
S4N9	168.38	7.09	23.75	$10.00 \times 0.31 \times 3.00$	90	T	101.89	0.714
S4N10	168.69	7.34	22.98	$10.00 \times 0.40 \times 3.00$	90	T	104.16	0.617
S4N11	168.18	7.60	22.13	$10.00 \times 0.40 \times 2.50$	90	C	101.38	0.227
S4N12	168.35	7.24	23.25	$20.00 \times 0.50 \times 2.20$	0	T	104.63	0.740
S4N13	168.24	7.43	22.64	$22.00 \times 0.25 \times 3.40$	0	C	96.38	0.250
S4N14	168.55	7.22	23.34	$20.00 \times 0.35 \times 1.50$	0	C	100.45	0.403

Table 9 The overview of specimens with combined damage (dimension unit: mm; damage size: $l_{(i)} \times w_{(i)} \times d_{(i)}$)

S.N.	D	t	D/t	Crack	Dent	Notch	Location	M_{cr} (kNm)	κ_{cr} (1/m)
S5N1	168.25	8.33	20.20	$44 \times 0.31 \times 0.70$	$110 \times 80 \times 10$	$44 \times 9.5 \times 3.0$	C	97.173	0.163
S5N2	168.80	7.60	22.21	$44 \times 0.31 \times 0.70$	$110 \times 80 \times 10$	$44 \times 10 \times 3.0$	C	85.72	0.153
S5N3	167.65	7.38	22.72	$45 \times 0.50 \times 0.70$	—	$45 \times 9.5 \times 3.0$	T	87.68	0.170
S5N4	167.37	7.15	23.41	$45 \times 0.53 \times 0.70$	—	$45 \times 10 \times 3.0$	T	85.98	0.224
S5N5	169.52	7.72	21.96	$37.5 \times 0.28 \times 0.70$	$78 \times 96 \times 8.5$	$44 \times 9.5 \times 3.5$	T	90.384	0.300

Appendix B: Moment–Curvature Diagrams of Specimens

This Appendix presents the results of specimens under bending test in the form of moment–curvature diagrams.
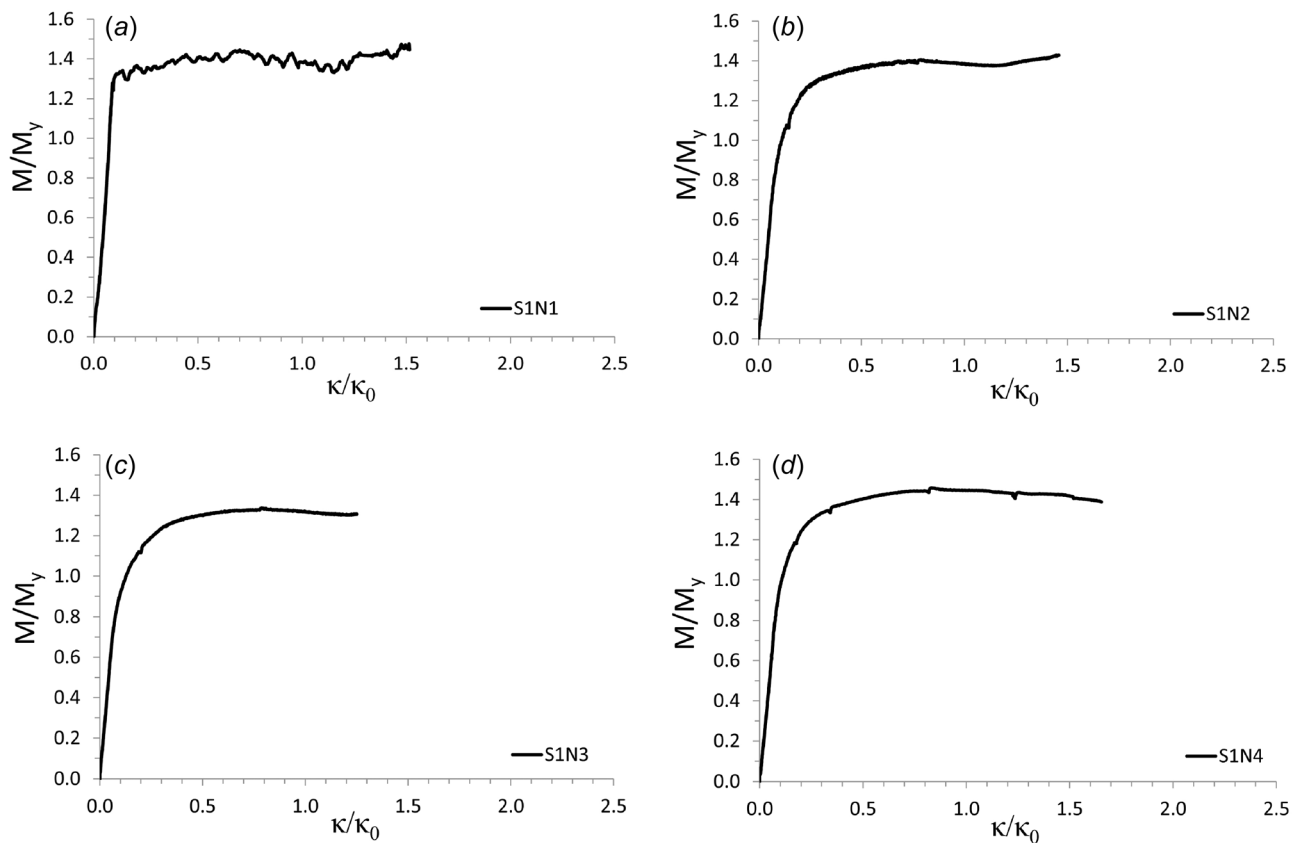

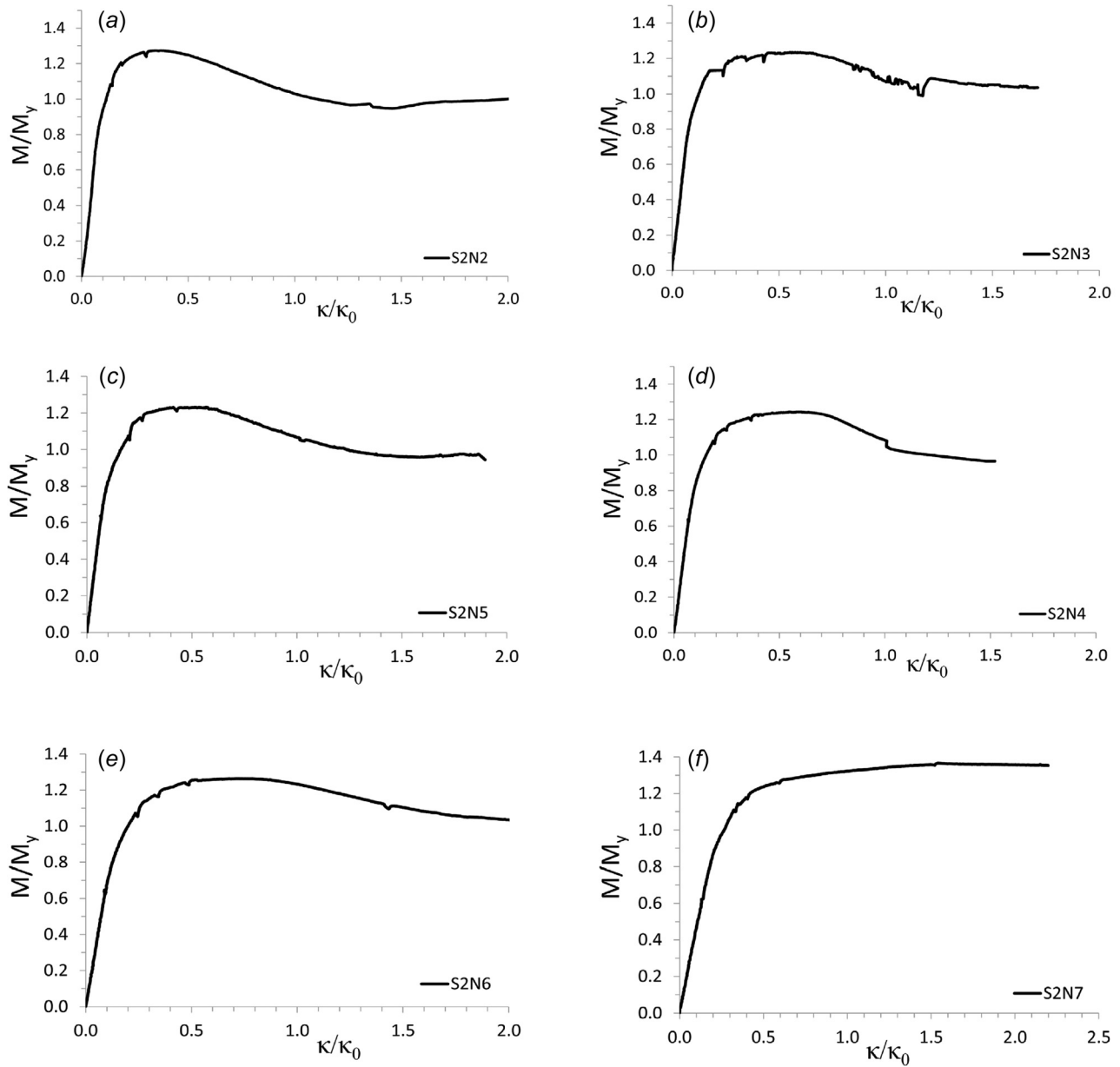**Fig. 21** Moment–curvature diagrams of intact specimens: (*a*) S1N1, (*b*) S1N2, (*c*) S1N3, and (*d*) S1N4

Fig. 22   Moment–curvature diagrams of dented specimens: (*a*) **S2N2 with a 90 deg dent,** (*b*) **S2N3 with a 45 deg dent,** (*c*) **S2N4 with a 0 deg dent,** (*d*) **S2N5 with a 90 deg dent,** (*e*) **S2N6 with a 90 deg dent, and** (*f*) **S2N7 with a 90 deg dent on the tensile side**
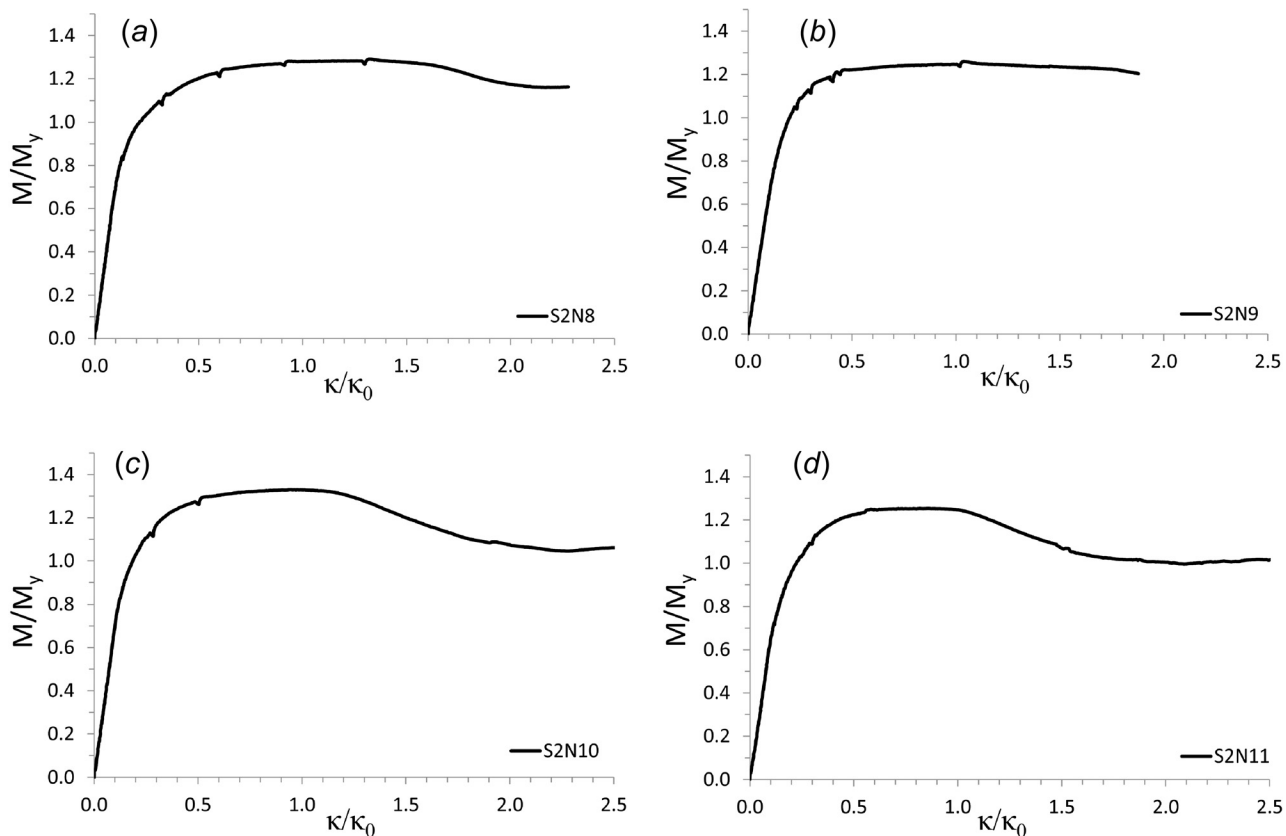
Fig. 23 Moment–curvature diagrams of specimens with impact-induced dent (all on the compression side): (a) S2N8 with a 90 deg dent, (b) S2N9 with a 90 deg dent, (c) S2N10 with a 90 deg dent, and (d) S2N11 with a 90 deg dent
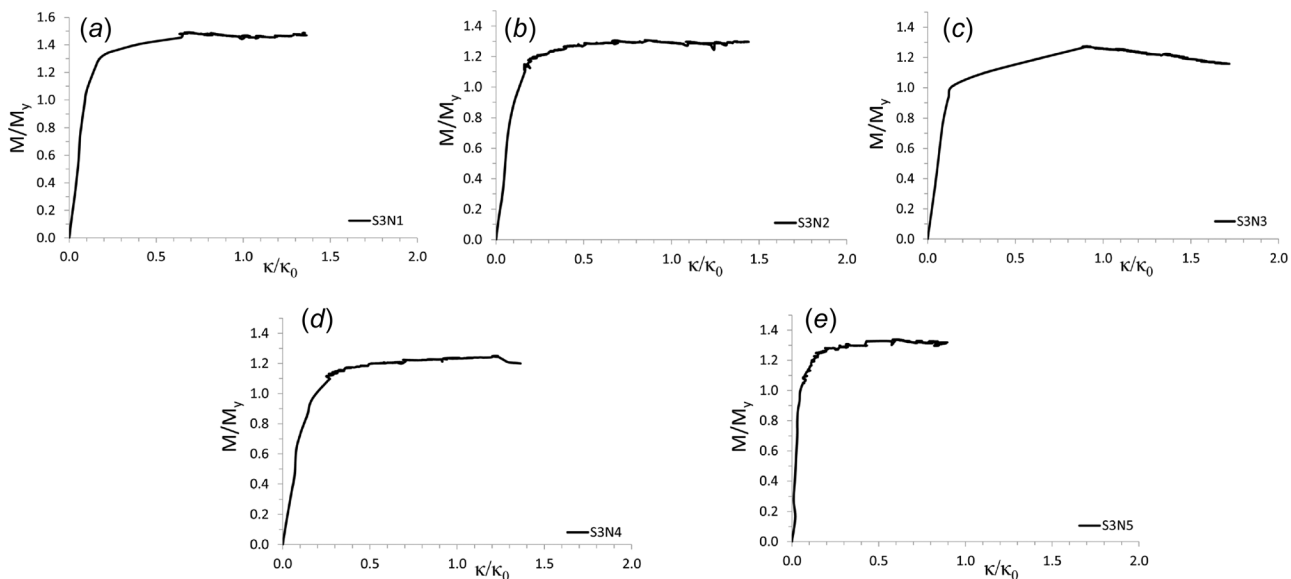

Fig. 24 Moment–curvature diagrams of specimens with metal loss damage: (a) S3N1 with metal loss on the compression side, (b) S3N2 with metal loss on the compression side, (c) S3N3 with metal loss on the compression side, (d) S3N4 with metal loss on the tensile side, and (e) S3N5 with metal loss on the tensile side
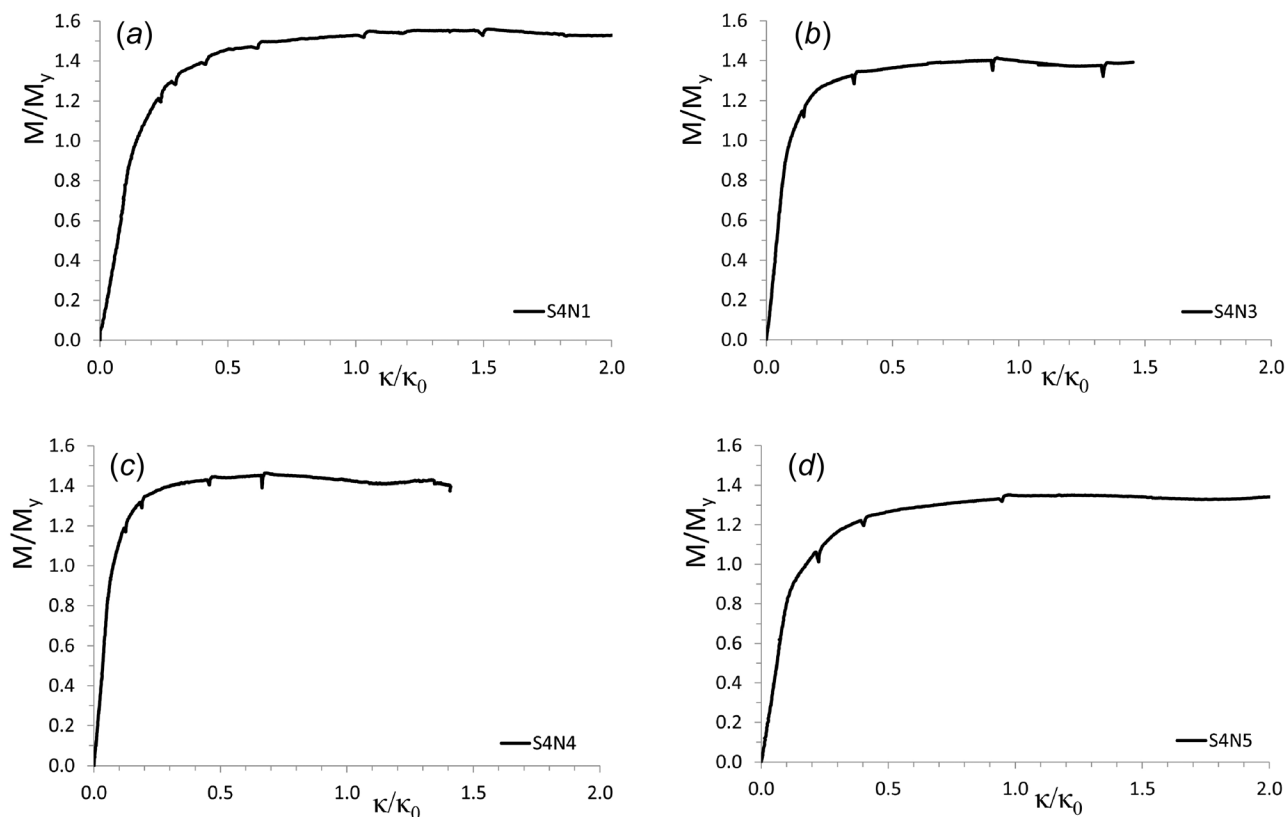
Fig. 25 Moment–curvature diagrams of specimens with shallow crack: (*a*) S4N1 with a crack in hoop direction on the tensile side, (*b*) S4N3 with a crack in hoop direction on the compression side, (*c*) S4N4 with a crack in longitudinal direction on the compression side, and (*d*) S4N5 with a longitudinal direction on the tensile side
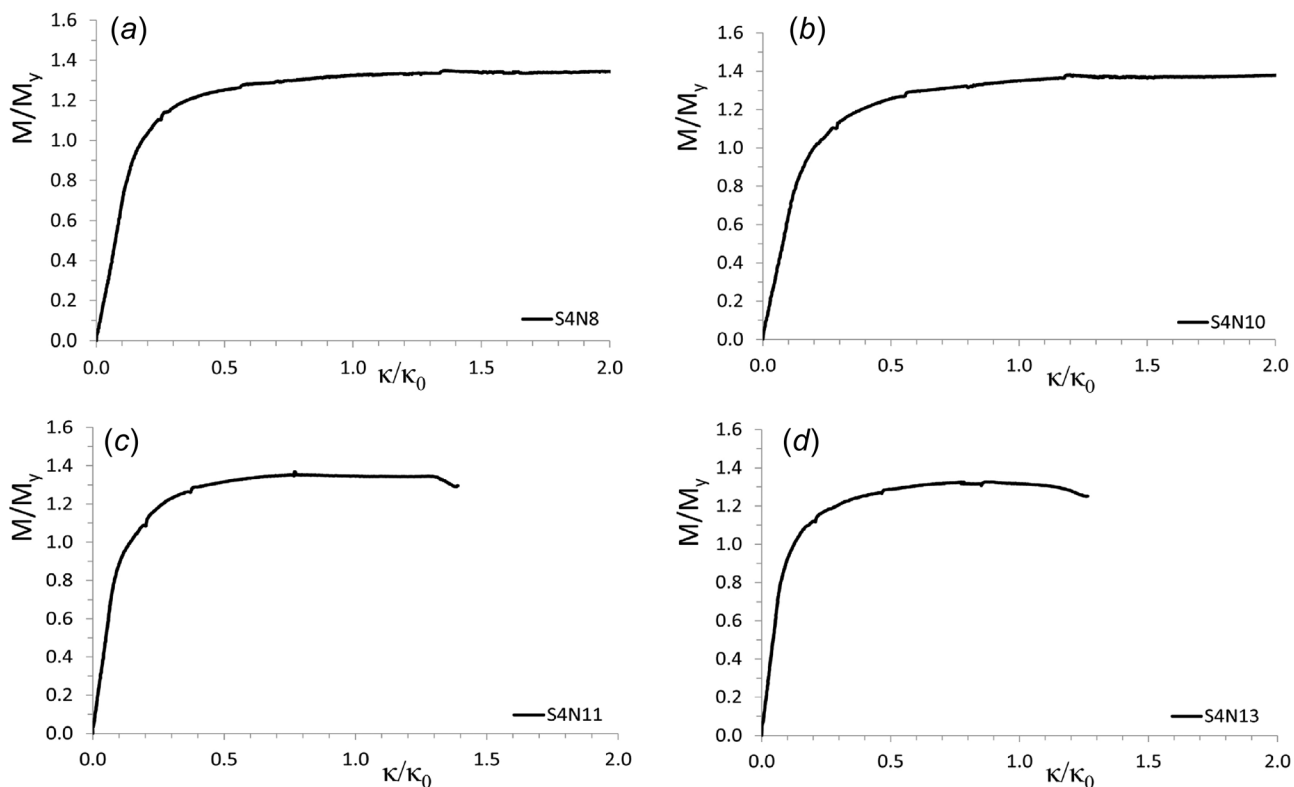

Fig. 26 Moment–curvature diagrams of specimens with deep crack: (*a*) S4N8 with a crack in hoop direction on the tensile side, (*b*) S4N10 with a crack in hoop direction on the tensile side, (*c*) S4N11 with a crack in hoop direction on the compression side, and (*d*) S4N13 with a crack in longitudinal direction on the compression side
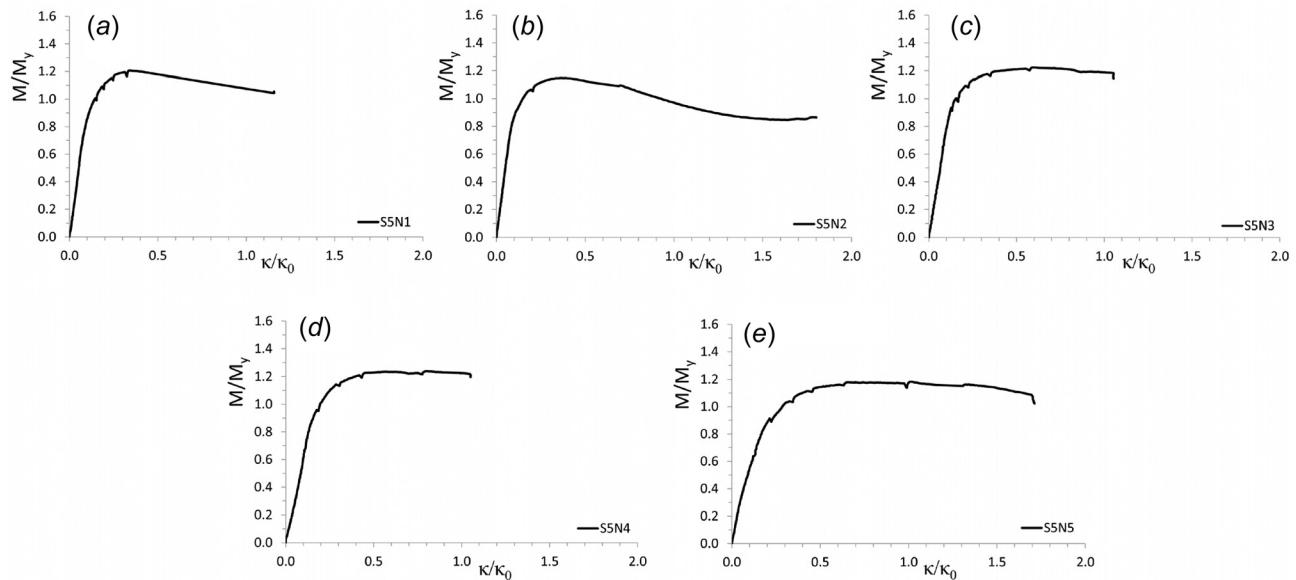
Fig. 27 Moment–curvature diagrams of specimens with combined damage: (*a*) S5N1 with combined dent, notch and crack on the compression side, (*b*) S5N2 with combined dent, notch and crack on the compression side, (*c*) S5N3 with combined notch and crack on the tensile side, (*d*) S5N4 with combined notch and crack on the tensile side, and (*e*) S5N5 with combined notch and crack on the tensile side

References

[1] Macdonald, K., and Cosham, A., 2005, "Best Practice for the Assessment of Defects in Pipelines–Gouges and Dents," Eng. Failure Anal., **12**(5), pp. 720–745.

[2] Ghaednia, H., Das, S., Wang, R., and Kania, R., 2015, "Safe Burst Strength of a Pipeline With Dent–Crack Defect: Effect of Crack Depth and Operating Pressure," Eng. Failure Anal., **55**(5), pp. 288–299.

[3] Fyrileiv, O., Aamlid, O., Venås, A., and Collberg, L., 2013, "Deepwater Pipelines–Status, Challenges and Future Trends," Proc. Inst. Mech. Eng., Part M, **227**(4), pp. 381–395.

[4] Guo, B., Song, S., and Ghalambor, A., 2013, *Offshore Pipelines: Design, Installation, and Maintenance*, Gulf Professional Publishing, Houston, TX.

[5] PHMSA, 2017, "Pipeline Incident 20 Year Trend," U.S. Department of Transportation, Washington, DC.

[6] Bjørnøy, O., Rengård, O., Fredheim, S., and Bruce, P., 2000, "Residual Strength of Dented Pipelines, DNV Test Results," Tenth International Offshore and Polar Engineering Conference, Seattle, WA, May 28–June 2, pp. 182–188.

[7] Bai, Y., and Bai, Q., 2014, *Subsea Pipeline Integrity and Risk Management*, Gulf Professional Publishing, Houston, TX.

[8] DNV, 2010, *DNV-RP-F111:Interference Between Trawl Gear and Pipelines*, Det Norske Veritas, Oslo, Norway.

[9] Abeele, F., Galvan, B., Ramos, P., and Muylle, J., 2013, "Numerical Simulation of the Interference Between Trawl Gear and Offshore Pipelines," Sixth International Pipeline Technology Conference, Ostend, Belgium, Oct. 7–9.

[10] DNV, 2013, *DNV-OS-F101* Submarine Pipeline Systems. Det Norske Veritas, Oslo, Norway.

[11] Vitali, L., Bartolini, L., Askheim, D., Peek, R., and Levold, E., 2005, "Hotpipe JI Project: Experimental Test and FE Analyses," ASME Paper No. OMAE2005-67526.

[12] Gresnigt, A., and Foeken, R. V., 2001, "Local Buckling of UOE and Seamless Steel Pipes," Eleventh International Offshore and Polar Engineering Conference, International Society of Offshore and Polar Engineers, Stavanger, Norway, Stavanger, Norway, June 17–22, pp. 131–142.

[13] Levold, E., Marchionni, L., Vitali, L., Molinari, C., Restelli, A., and Ozkan, I. F., 2013, "Strength and Deformation Capacity of Corroded Pipe–Laboratory Tests and FEM Analyses," Twenty-Third International Offshore and Polar Engineering Conference, International Society of Offshore and Polar Engineers, Anchorage, AK, June 30–July 5, pp. 1–9.

[14] Netto, T., Ferraz, U., and Botto, A., 2006, "Residual Strength of Corroded Pipelines Under External Pressure: A Simple Assessment," International Pipeline Conference, American Society of Mechanical Engineers, AB, Canada, Sept. 25–29, pp. 143–156.

[15] Hilberink, A., 2011, "Mechanical Behaviour of Lined Pipe," Ph.D. thesis, Delft University of Technology, Delft, The Netherlands.

[16] Smith, C., Somerville, W., and Swan, J., 1981, "Residual Strength and Stiffness of Damaged Steel Bracing Members," Offshore Technology Conference, Offshore Technology Conference, Houston, TX, May 4–7, pp. 273–283.

[17] Taby, J., Moan, T., and Rashed, S., 1981, "Theoretical and Experimental Study of the Behaviour of Damaged Tubular Members in Offshore Structures," Norwegian Marit. Res., **9**(2), pp. 26–33.

[18] Kyriakides, S., Babcock, C., and Elyada, D., 1984, "Initiation of Propagating Buckles From Local Pipeline Damages," ASME J. Energy Resour. Technol., **106**(1), pp. 79–87.

[19] Park, T., and Kyriakides, S., 1996, "On the Collapse of Dented Cylinders Under External Pressure," Int. J. Mech. Sci., **38**(5), pp. 557–578.

[20] Ellinas, C. P., 1984, "Ultimate Strength of Damaged Tubular Bracing Members," J. Struct. Eng., **110**(2), pp. 245–259.

[21] Bai, Y., Igland, R. T., and Moan, T., 1994, "Ultimate Limit States of Pipes Under Tension and Bending," Int. J. Offshore Polar Eng., **4**(4), pp. 312–319.

[22] Hauch, S., and Bai, Y., 2000, "Bending Moment Capacity of Groove Corroded Pipes," Tenth International Offshore and Polar Engineering Conference, International Society of Offshore and Polar Engineers, Seattle, WA, May 28–June 2, pp. 253–263.

[23] Guarracino, F., Walker, A., and Giordano, A., 2009, "Effects of Boundary Conditions on Testing of Pipes and Finite Element Modelling," Int. J. Pressure Vessels Piping, **86**(2–3), pp. 196–206.

[24] Es, S., Gresnigt, A., Vasilikis, D., and Karamanos, S., 2016, "Ultimate Bending Capacity of Spiral–Welded Steel Tubes–Part I: Experiments," Thin-Walled Struct., **102**, pp. 286–304.

[25] Cai, J., Jiang, X., and Lodewijks, G., 2016, "Residual Strength of Metallic Pipelines Subject to Combined Loads Accounting for Impact Induced Damage," 26th International Ocean and Polar Engineering Conference, International Society of Offshore and Polar Engineers, Rhodes, Greece, June 26–July 2, pp. 335–341.

[26] Cai, J., Jiang, X., and Lodewijks, G., 2017, "Residual Ultimate Strength of Offshore Metallic Pipelines With Structural Damage–a Literature Review," Ships Offshore Struct., **12**(8), pp. 1037–1055.

[27] Cai, J., Jiang, X., Lodewijks, G., Pei, Z., and Wu, W., 2018, "Residual Ultimate Strength of Seamless Metallic Pipelines Under a Bending Moment—A Numerical Investigation," Ocean Eng., **164**, pp. 148–159.

[28] Cai, J., Jiang, X., Lodewijks, G., Pei, Z., and Wu, W., 2018, "Residual Ultimate Strength of Damaged Seamless Metallic Pipelines With Combined Dent and Metal Loss," Mar. Struct., **61**, pp. 188–201.

[29] Ghazijahani, T. G., Jiao, H., and Holloway, D., 2015, "Experiments on Dented Steel Tubes Under Bending," Adv. Struct. Eng., **18**(11), pp. 1807–1817.

[30] Chinese Standard, 2008, "High Strength Low Alloy Structural Steels (in Chinese)," The Chinese National Standard, Beijing, China, Standard No. GB/T 1591.

[31] Chinese Standard, 2008, "Metallic Materials-Tensile Testing—Part:1 Method of Test at Room Temperature (in Chinese)," The Chinese National Standard, Beijing, China, Standard No. GB/T 228.1.

[32] Zhao, K., Wang, L., Chang, y., and Yan, J., 2016, "Identification of Post-Necking Stress-Strain Curve for Sheet Metals by Inverse Method," Mech. Mater., **92**, pp. 107–118.

[33] Thinvongpituk, C., Poonaya, S., Choksawadee, S., and Lee, M., 2008, "The Ovalisation of Thin-Walled Circular Tubes Subjected to Bending," World Congress on Engineering, London, U.K., July 2–4, pp. 2–4.

[34] Dimopoulos, C., and Gantes, C., 2013, "Comparison of Stiffening Types of the Cutout in Tubular Wind Turbine Towers," J. Constr. Steel Res., **83**, pp. 62–74.

[35] European Committee for Standardization, 2006, *Eurocode 3: Design of Steel Structures—Part 1-1: General Rules for Buildings*, European Committee for Standardization, Belgium, Brussels.

[36] Cai, J., Jiang, X., and Lodewijks, G., 2018, "Numerical Investigation of Residual Ultimate Strength of Dented Metallic Pipes Subjected to Pure Bending," Ships Offshore Struct., **13**(5), pp. 519–531.

[37] Cai, J., Jiang, X., Lodewijks, G., Pei, Z., and Wu, W., 2018, "Residual Ultimate Strength of Damaged Seamless Metallic Pipelines With Metal Loss," Mar. Struct., **58**, pp. 242–253.

[38] Miraoui, I., Boujelbene, M., and Zaied, M., 2016, "High-Power Laser Cutting of Steel Plates: Heat Affected Zone Analysis," Adv. Mater. Sci. Eng., **2016**, p. 8.